Study of the Ability of Multiphase Continuum Models to Predict Core-Annulus Flow

Sofiane Benyahia
Fluent Incorporated, Morgantown, WV 26505

Madhava Syamlal and Thomas J. O'Brien
National Energy Technology Laboratory, Morgantown, WV 26505

DOI 10.1002/aic.11276
Published online August 10, 2007 in Wiley InterScience (www.interscience.wiley.com).

We use the well established core-annulus flow regime as a numerical benchmark to evaluate the sensitivity of gas–solids continuum models and boundary conditions to model formalisms and parameters. By using transient, 1D, grid-independent numerical solutions, we avoid the use of speculative closure terms and show that the kinetic theory of granular flow (KTGF) is sufficient to model core-annulus regime. That regime arises in the time-average solution as a consequence of the fluctuating motion of regions with high solids concentration. These fluctuations are most sensitive to the gravitational acceleration (g) and granular energy dissipation terms. The fluctuation frequency is $\alpha\sqrt{g}$*. The effect of fluctuations is so dominant that decreasing the restitution coefficient (KTGF parameter) actually increases the average granular temperature. The wall boundary conditions for solids momentum and granular energy equations dictate the core-annulus flow regime. They must cause a net dissipation of granular energy at the wall for predicting that regime.* © 2007 American Institute of Chemical Engineers* *AIChE J,* 53: 2549–2568, 2007
Keywords: particulate flows, computational fluid dynamics (CFD), fluidization, mathematical modeling, turbulence

Introduction

Core-annulus flow is an experimentally well established, industrially significant flow regime found in circulating fluidized beds, such as fluid catalytic cracking and coal gasification processes; particles tend to segregate into clusters and streamers that migrate to the walls, thus forming a dense annulus and a dilute core.[1–4] (By clusters, we mean transient dense flow regions that may have different shapes in 1D (one-dimensional) and 2D. The size of these clusters can be of the same order of magnitude as the system geometry and may be different from what is typically called "cluster" in the literature.) This is a transient phenomenon; clusters and streamers forming near the walls have very short lifetimes (see the excellent review by Bhusarapu et al.[5]). The accurate prediction of this regime has been the objective of many modeling studies and multiphase continuum models are able to predict core-annulus flow. Although granular kinetic theory has been widely accepted as an essential constitutive model for simulating this flow regime, the role of gas–solids turbulence models, boundary conditions (BC), and model parameters in predicting core-annulus flow is not well understood. To evaluate their role, we use the core-annulus flow regime as a sine qua non numerical benchmark; we determine the model features and parameters that affect the model's ability to predict core-annulus flow. We do not intend to compare with experimental data or conduct validation studies because we are not proposing any new models. All the continuum models and BC were previously published in peer reviewed journals. Furthermore, the flow condition used in this study fall within a wide range of operating conditions under which core-annulus flow is known to occur.[6]

Correspondence concerning this article should be addressed to S. Benyahia at this current address: National Energy Technology Laboratory, Morgantown, WV 26505; e-mail: sofiane.benyahia@netl.doe.gov.

Sinclair and Jackson[7] used the kinetic theory of granular flow (KTGF) in a steady-state, 1D (vertical) model to investigate the flow regimes in a tube and demonstrated that the solids concentration was inversely proportional to the granular temperature (or kinetic energy of particle fluctuations). Pita and Sundaresan[8] showed that this model manifested an "unrealistic sensitivity" to the inelasticity of particle–particle collisions. Yasuna et al.[9] showed very good agreement between experimental data and the calculated solids fraction distribution by assuming perfectly elastic collisions. Reducing the restitution coefficient to a value of 0.99, however, reversed the flow structure; the granular temperature was lowest and the solids concentration was the highest at the center. This sensitivity is clearly unrealistic because the particle–particle restitution coefficient is usually between 0.9 and 0.95.[10–12] Tsuo and Gidaspow[13] showed that cluster formation can be numerically predicted by transient continuum models, even using a simple correlation for the solids viscosity rather than that calculated from KTGF.

Pita and Sundaresan[8] showed that the steady-state model also manifests an unrealistic sensitivity to the dampening of the fluctuating motion of the particles by the gas. For that dissipation term in the granular energy equation, they used $3\beta\Theta_s$, derived by Ding and Gidaspow[14] and subsequently used by Cao and Ahmadi,[15] Balzer et al.,[16] and Agrawal et al.[17] The addition of this sink term prevents the prediction of a core-annulus flow regime even when the restitution coefficient is unity.

This unrealistic sensitivity to the restitution coefficient and the $3\beta\Theta_s$ term is caused by the assumption of steady state without introducing terms to account for the effects of time-smoothing. Now it is well understood that the core-annulus structure arises, in a time-averaged sense, from the dynamics of the unsteady motion. Steady-state equations obtained by simply dropping the transient term, without accounting for their effect through constitutive laws, are not adequate. This was first recognized by Dasgupta et al.,[18] who developed time-smoothed equations and used speculative closures for the correlation terms that appear in such equations. They did not include constitutive equations from KTGF, however. Hrenya and Sinclair[19] included KTGF, as well as closures for the correlation terms, to derive a time-smoothed form of the Sinclair and Jackson model, which is not unrealistically sensitive to the restitution coefficient. For example, they were able to predict core-annulus flow even with a restitution coefficient as low as 0.9. Although the issue of undue sensitivity to restitution coefficient is now settled, there is no demonstration in the literature of the role of the restitution coefficient without resorting to speculative closure terms in a time-steady model. One objective of this article is to examine this feature by using grid-independent transient simulations that do not require the use of any speculative closure terms.

Another physical phenomenon that potentially has an effect on the core-annulus structure is gas phase turbulence. Since gas phase turbulence is usually suppressed in heavily-loaded flows, it could have a significant effect on dilute gas solids flows and a negligible effect on dense gas solids flows.[20] We have investigated three different gas/solids turbulence models published in the literature. Two of these models, Balzer et al.[16] and Cao and Ahmadi,[15] account for the effect of gas turbulence through the use of a modified $k-\varepsilon$ model, whereas Agrawal et al.[17] does not model the gas-phase turbulence at all, only that of the granular phase. Balzer et al. and Agrawal et al. both use similar modifications to the solids granular viscosity and conductivity to include the effect of the gas phase in dilute flows, whereas Cao and Ahmadi use the "dry" granular kinetic theory. Although the results of these models have been published, here we present the results of mesh-resolved simulations with the three models implemented consistently using the same open-source software, MFIX. Thus, differences in the predictions can be traced directly to differences in the physical models without concern about numerical issues. Under the flow regime used in this study, the gas phase turbulent stresses could be neglected without any effect on the predicted time-averaged flow results.

In addition, several wall BC have been proposed for the continuum gas–solids flow equations. The core-annulus flow is strongly affected by the particle/wall friction coefficient. We compare the effect of three wall BC in this study: Johnson and Jackson,[21] Jenkins,[22] and free slip for solids velocity with a specified granular temperature of zero at the wall. The Johnson and Jackson wall BC[7,21,23,24] for solids velocity and granular temperature uses a specularity coefficient that describes the roughness of the wall; a value of zero refers to perfectly specular collisions (smooth) and a value of unity refers to perfectly diffuse (rough) collisions.[23,25] Unfortunately the specularity coefficient is difficult to measure. Experimental values of specularity coefficient have not been reported to the best of our knowledge. Shaffer et al.[12] (a reference pointed out by a reviewer) used a controlled environment with a fixed velocity and angular impact to measure particle-wall restitution and friction coefficients. Measurements in an operating riser to obtain meaningful values of the specularity coefficient appear unattainable. Nevertheless, different values of the specularity coefficient have been used in the literature without a clear explanation of their choice.[7,23,26] We will explain in this article why the values of specularity coefficient typically used in steady state simulations to compute core-annulus flow regime are not suitable for transient simulations.

Jenkins[22] BC have been used in other studies.[15,27] He reported two limits (low friction and high friction) depending on whether the particles are assumed to slide (low friction) or bounce back tangentially (high friction) during collisions with walls. Benyahia et al.[27] showed that the high friction limit BC causes unrealistically large granular energy production at the wall. Therefore, in this study we use only the low friction (sliding) condition. An analysis of this condition shows that it can predict either the production or the consumption of granular energy at the wall (source or sink) depending on the value of particle-wall restitution coefficient and friction coefficient. Thus, there is a value of the friction coefficient above which there is sufficient production of granular energy to cause the solids to be pushed away from the walls. To predict the build up of particle concentration near the wall, the value of the friction coefficient needs to be small, which is in agreement with previous studies.[16,23,27,28] This observation motivated the evaluation of a third BC: free slip BC for the solids velocity and a specified value of zero for the granular temperature at the walls.

For turbulent flows, the wall BC for the fluid phase are either approximated by wall functions or imposed by fully

resolving the flow near the wall. Several authors[15,16,29] used a refined computational mesh to resolve the turbulent boundary layer near the walls. With a coarser mesh, De Wilde et al.[30] used wall functions, common in single phase turbulent flows. The single phase wall functions were extended[27] by including the contribution of exchange of turbulent energy because of gas–solids momentum exchange although this had little effect on the flow patterns for dilute flows. For the moderately dense flows studied here, the effect of the modified wall function is also negligible.

The simulations give steady state solutions at zero gravity. Unexpectedly, we also found that a steady state solution can be obtained by setting all the dissipation terms in the granular energy equation to zero.

Gas–Solids Flow Continuum Models

The continuum model equations used in the present study are summarized in Tables A1 and A2 in the appendix. The primary model used in this study is described in detail by Agrawal et al.[17] and will be called the A-model in the rest of this article. Two additional models are also studied: B-model (Balzer et al.[16]) and C-model (Cao and Ahmadi[15]). All three models use the KTGF. In addition, the B- and C-models solve for the turbulence in the gas phase, using a modified $k - \varepsilon$ theory, derived from single-phase turbulence theory but including terms that account for the exchange of turbulence energy between the fluid and solids phases. The B-model contains a term in the gas turbulence energy dissipation (ε) equation to account for the extra dissipation caused by the solids phase (see Table A2); that term is absent in the C-model. The description of the dissipation of granular energy due to turbulence energy exchange is identical in both models. However, the expressions for solids conductivity and viscosity are slightly different. The A- and B-models both include modifications to the solids viscosity and conductivity to account for the presence of the fluid; the C-model uses the "dry" granular kinetic theory without such modifications. Another difference between these models is in the turbulent energy exchange terms. The sink term[31] in the granular energy equation, $3\beta\Theta_s$, is the same in all the models; however, the source term is different (see Eqs. A25–A28). The A-model uses an adjustable parameter in the shear stress; the value used in this study ($\alpha = 1.6$) was obtained[21] by fitting the model predictions to experimental data.

There are other differences that are less important for the moderately dense gas/solids flows investigated in this study. For example, the B-model introduces a new dissipation timescale, $\frac{1}{\tau_2} = \frac{2}{\tau_{12}^{\varepsilon}} + \frac{\sigma_c}{\tau_2^c}$, which combines the particle relaxation and collisional time scales (Table A2). This harmonic combination goes to the correct limits with respect to the solids volume fraction—for very dilute systems, the main dissipation is due to the drag interaction between the fluid and particles; for denser systems, particle–particle collisions are the dominate dissipation mechanism.[27] This approach avoids the use of an ad hoc limit to the solids viscosity for very dilute flows.[27] A similar combination of time scales is used in the A-model, but not in the C-model.

All the simulations were conducted with the well known Wen and Yu drag correlation.[17,31] This drag correlation was shown[32] to compare well with lattice-Boltzmann simulation data, especially for solids volume fractions less than 0.3. Frictional granular stress models[33] are not needed because the flows studied here are not in the frictional flow regime. The Carnahan and Starling radial distribution function at contact was used in this study (see van Wachem et al.[34] for a discussion).

The wall boundary conditions (BC) are from Jenkins[22] and Johnson and Jackson[21] (Table A3). As mentioned, only the low frictional version of Jenkins' BC is used in this study. We also examine a free slip BC for solids velocity with a specified (zero) value for granular temperature at the walls.

For the gas phase wall BC, standard and modified wall functions are used with the B-model. Modifications to the wall functions are presented in Table A3 and include the effect of the solids phase because of fluid-solids turbulent kinetic energy exchange. As is typical of wall function implementations, these modifications are only included in the production and dissipation of the fluid turbulent kinetic energy in the cells adjacent to walls.[27] With C-model, we used only standard wall functions. With the A-model, a no-slip condition was used in most simulations except when a free slip was used for the solids phase, in which case a free slip condition was also used for the gas phase. These different BC for the gas phase caused only minor differences in the predicted gas/solids flow patterns as we will demonstrate later in this article.

The open source software MFIX was used for solving the model equations (http://www.mfix.org/). The current set of equations programmed in the software is given in Benyahia et al.[35]; an earlier version is described in Syamlal et al.[36] The numerical technique is described in Syamlal.[37]

Simulation Conditions

A parametric sensitivity analysis with respect to particle–particle restitution coefficient and particle-wall friction coefficient was conducted. We report the simulation results for the isothermal flow of air and glass beads in a vertical channel of 0.1 m width (horizontal). The domain is 1D (horizontal) with periodic BC and a pressure drop in the vertical direction. We solve for both the vertical (only one computational cell is used in the vertical direction) and horizontal components of the velocity field. All variables are functions of horizontal position and time only. A superficial (vertical) gas velocity of 5.5 m/s and an average solids volume fraction of 0.03 are used in all these simulations. A constant gas mass flux of 6.52 kg/(m^2 s) is prescribed to achieve this superficial gas velocity. The gas pressure drop is adjusted to maintain this constant gas mass flux, within a tolerance of less than 10^{-2} kg/(m^2 s). (Reducing this tolerance reduces the small fluctuations in pressure drop, but does not change the time-averaged results.) The physical properties of the gas (air) and solids are presented in Table 1. The gas density is calculated using the ideal gas law.

The numerical residuals of all equations are set to 10^{-4}, and the gas and solids pressure correction residuals are normalized using the first iteration residual at each time step. Lowering the residual tolerance has only a small effect on the time-averaged results presented in this study, but results in a significant increase in CPU time. An adaptive time stepping procedure based on minimizing the number of nonlinear iterations per second of simulation time was used in

Table 1. Physical Parameters Used in this Study

Process temperature	298 K
Process pressure	101,325 Pa
Air density	Computed using ideal gas law (about 1.2 kg/m^3)
Air viscosity	1.8×10^{-5} Pa s
Solids density	2400 kg/m^3
Particle diameter	0.012 cm
Particle–particle restitution coefficient	0.95 (other values were also used and will be mentioned in the text)
Particle-wall restitution coefficient	0.7
Particle-wall friction coefficient	0.2 and 0.3
Specularity coefficient	0.003 and 0.001

this study. The average time step was typically of the order of 10^{-4} s.

Uniform initial conditions are prescribed for all the simulation cases. Initially, a uniform solids volume fraction of 0.03 is set. Also, across the 0.1 m width, the initial solids and gas vertical velocities are 5.2 and 5.5 m/s, respectively; the initial horizontal gas and solids velocity are set to zero for all cases. The initial granular temperature is 0.1 m^2/s^2 and the gas turbulent energy and dissipation are set (in case the $k - \varepsilon$ model is used) to 0.01 m^2/s^2 and 0.1 m^2/s^3, respectively. Ambient gas pressure and temperature are used in all simulation cases, 298 K and 101 kPa. These conditions fall within a wide range of operating conditions under which core-annulus flow is known to occur.[6]

We study a horizontal 1D system with periodic flow in the vertical direction for reasons of computational economy and simplicity in analyzing the results. Other studies have examined vertical 1D solutions to continuum models,[7,8,15,19,26] a distinguishing feature of our study is the transient nature of the simulations. We wish to emphasize that studying a 1D system can shed light on various features of the continuum model, but not all (e.g., effects of inlets and outlets and recirculation can not be captured). Thus, it cannot be used for quantitative comparison with experimental data and, therefore, we do not make such comparisons. However, such effects do not dictate cluster formation and the consequent establishment of core-annulus flow.[28] Also, preliminary results of much more computationally intensive 2D periodic simulations are qualitatively similar to those of 1D simulations (core-annulus structure occurs in both 1D and 2D systems), although there are quantitative differences.[38] The qualitative effects are presumably valid in 3D systems as well. Also, the relatively low CPU time required for 1D simulations allowed us to investigate the effect of model parameters extensively, yet economically.

Grid Independence

It is important to conduct a grid refinement study to show that the numerical solution is independent of the grid size. This concept has meaning only when the criteria of convergence are clearly and quantitatively defined. In this study we take two criteria for grid convergence: first, the time averaged profiles of solids volume fraction, gas and solids velocities and granular temperature, and second, the transient profiles of gas volume fraction at a location near the wall.

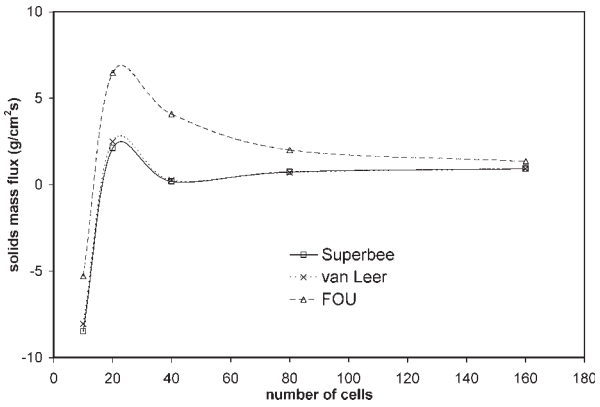

Figure 1. Effect of grid density for three numerical schemes (first order upwind or FOU, Superbee and van Leer) on the averaged solids mass flux.

Grid-converged numerical solutions are obtained with 80 computational cells for the second-order schemes (Superbee and van Leer).

Five numerical grid sizes were used in the grid refinement of the width of the 1D channel. The number of uniform computational cells required to consistently resolve the features discussed in this article was identified as 80, which is the number used for the remainder of the study. Three numerical schemes were used to discretize the convection terms: first-

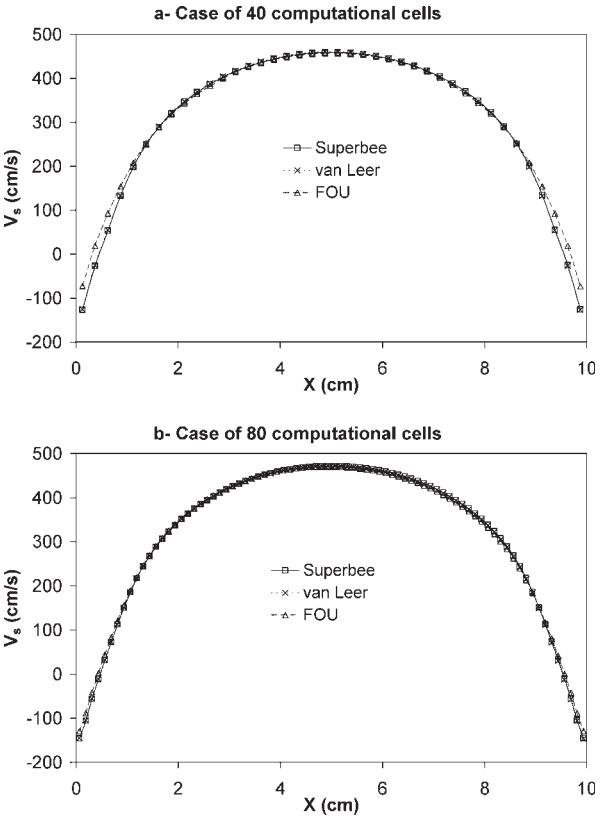

Figure 2. Time-averaged solids velocity profiles across the width of the channel, using the three numerical schemes and two grid resolutions (40 and 80 computational cells).

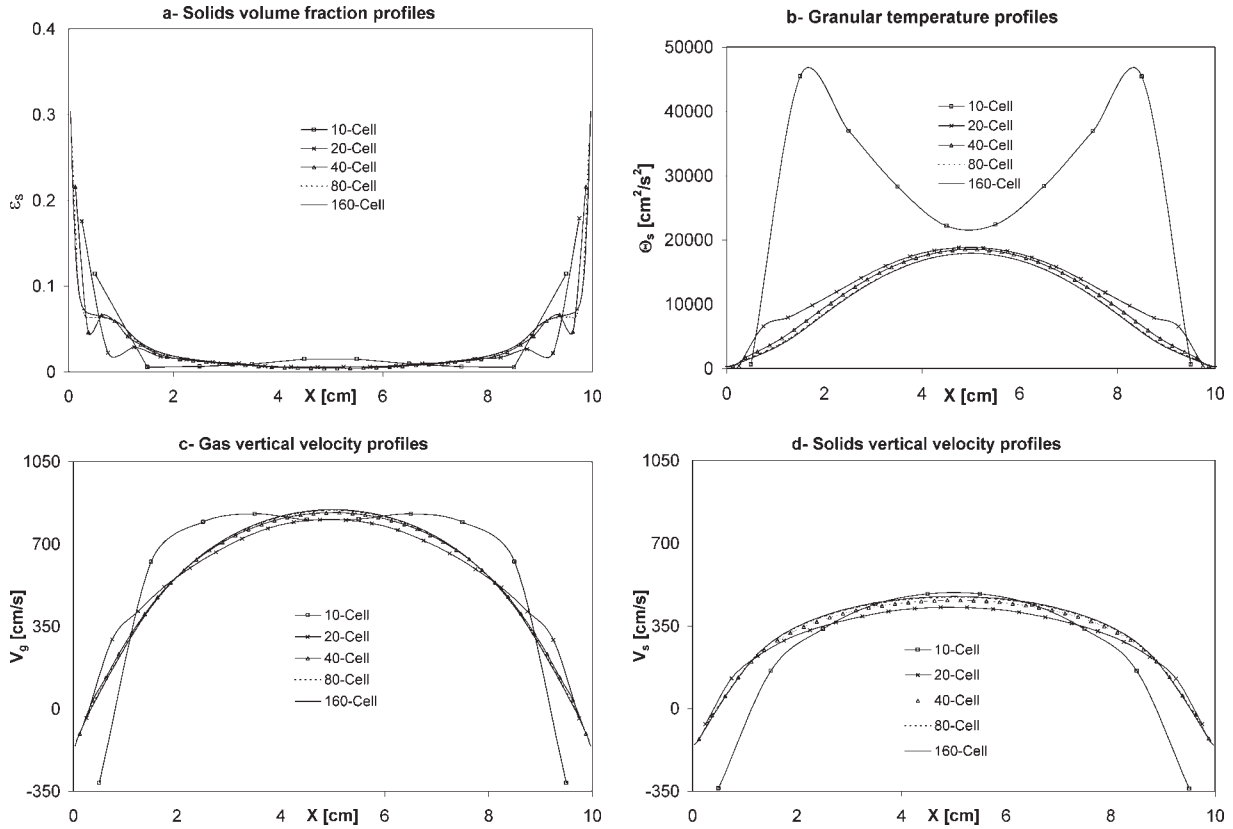

Figure 3. Time-averaged flow variables (solids volume fraction, granular temperature, and gas and solids velocities) profiles across the width of the channel for five numerical grid resolutions using the Superbee discretization scheme.

order upwind (FOU) and two high resolution (second-order) schemes, van Leer and Superbee. These schemes for multiphase flow are described in detail by Syamlal[37] and Guenther and Syamlal.[39] The simulations were conducted for 60 s, and the results of the last 45–50 s were time-averaged. The averaging time period was chosen such that the profiles are symmetric. Figure 1 shows the time-averaged total solids mass flux variation with the number of computational cells. This demonstrates that high resolution schemes converge faster to the grid independent solution than FOU. With high resolution schemes a grid-independent solids mass flux value could be reached at a grid size of 80, whereas FOU required a grid size of 160. Clearly, all three discretization schemes eventually converge to the same grid-independent solution.

Although for a given grid size second-order numerical schemes, such as Superbee or van Leer, are computationally more expensive than FOU, to obtain a given solution accuracy they are less expensive than FOU, which requires much higher grid refinement to attain the specified accuracy.[39] For example, in our calculations, a 160-cell run with FOU took about 31 h of CPU time (using Intel Xeon 3.0 GHz). A solution of comparable accuracy was obtained with the Superbee scheme and 80-cells, which took only about 8 h of CPU time. However, the CPU time using the Superbee scheme and 160-cells is about 46 h. For the same grid, the Superbee scheme was slower to converge because of many failed time-steps (time-steps that didn't converge to required tolerance), which caused about 13% of wasted nonlinear iterations for the 80-cells case.

Figure 1 shows that the coarse grid of 10-cells gives a solution that is even qualitatively wrong (the predicted flux is negative.) A coarse grid such as this (10-cells for a 10-cm channel) is not atypical of industrial simulations.[17] Clearly, grid independence needs to be established, before we can have confidence even in the qualitative trends predicted by a simulation.

Figure 2 shows the time-averaged solids vertical velocity profiles using 40 and 80 cells. The FOU scheme predicts almost the same profile as the two high resolution schemes. However, the clusters forming near the walls, which cause the solids to flow downward, are not predicted accurately using the FOU scheme. For the case of 40 cells the solids velocity near the walls predicted by FOU is not as negative as the grid-converged, higher order solutions. When the number of cells is increased from 40 to 80, FOU gives results that are in better agreement with the results of high resolution schemes. Figures 1 and 2 also show that only minor differences exist between the two high resolution schemes, Superbee and van Leer.

Figure 3 shows time-averaged profiles of four variables obtained with different grid sizes and the Superbee discretization scheme. All the profiles become grid-independent for 80 cells. It is not surprising that the solution obtained with the coarsest grid (10 cells) deviates the most from the grid-independent solution. But surprisingly the solution is even qualitatively incorrect: the solids concentration has a small local maximum at the center (Figure 3a), the granular tem-

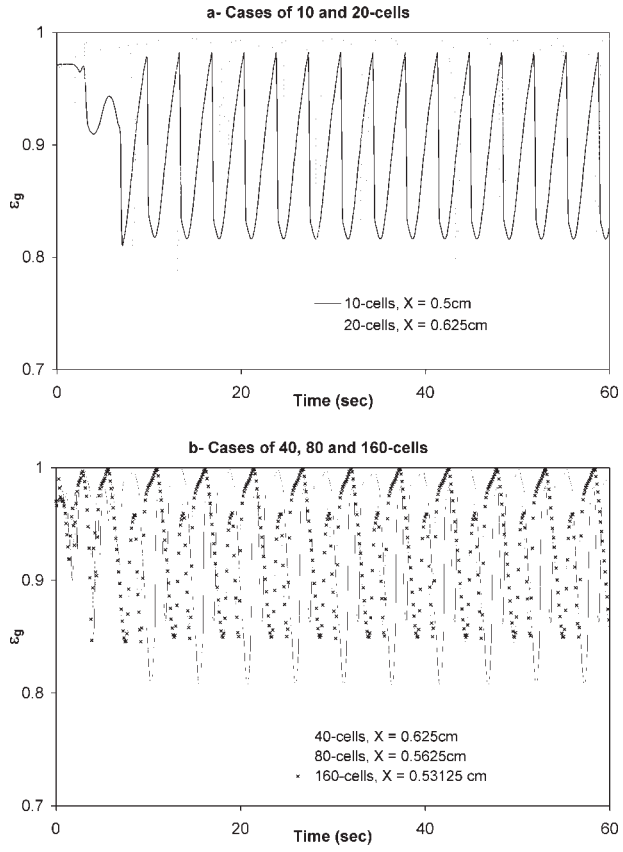

Figure 4. Transient profiles of void fraction near the wall for five numerical grid resolutions using the Superbee discretization scheme.

perature is considerably larger with peaks away from the center (Figure 3b), the maximum gas velocity is away from the center (Figure 3c), and the solids velocity attains large negative values near the wall (Figure 3d). The solutions obtained with grid sizes of 80 and 160 are nearly identical. Therefore, a grid of 80 cells, using the Superbee scheme, assures grid-independent solutions with respect to these properties. We use this combination of grid size and discretization scheme in the rest of this study. It is remarkable that with a grid size of 80 cells the size of the cells is about 10 times the particle diameter. This is in agreement with the reported[28,40] conditions for grid independence.

The numerical solutions from coarse grids may lead one to misinterpret the significance of various terms in the differential equation model. For example, Figure 3a shows that for the coarsest grid, the solids concentration increases at the core of the channel. This may explain why in a previous study, using a coarse grid,[24] it was necessary to omit a sink term in the granular energy equation ($3\beta\Theta_s$) to compute core-annulus flow.

The records of gas volume fraction as a function of time at a fixed location are shown in Figure 4 for different grid sizes, using Superbee. The location of this "probe" is about 0.55 cm from the wall (as indicated in the legend by X, the distance from wall), in the region where clusters form. An oscillatory profile is obtained after an initial transient period of 10 s. To give the reader more insight into the transient gas/solids flow dynamics we have created an animation of gas volume fraction and solids and gas velocity vectors (dilute and dense transient flow regions are indicated by blue and red colors, respectively), which is available at http://www.mfix.org/results/1-D.avi. The fine meshes of 160 and 80 cells give "identical" signals with a frequency of 0.188 Hz. The mesh of 40 cells gives a frequency of 0.192 Hz. The frequency of oscillations given by the 20 cells and 10 cells is 0.066 and 0.286, respectively; the pattern in these cases is quantitatively and qualitatively different from the grid-converged solution. In contrast, we found that the numerical solutions obtained using the fine meshes of 80 and 160 gave not only identical time-averaged solutions but also the same numerical solution at every instant (Figure 4b) The grid-independent value of 0.188 Hz is in the range of the frequency of oscillations commonly observed in riser simulations.[23,24]

Evaluation of Gas/Solids Turbulence Models

Figure 5 shows the time-averaged flow variables across the width of the 1D channel calculated using the A-, B-, and C-models. Similar core-annulus flow profiles are predicted using all three models. The highest concentration of solids at the walls is predicted by the A-model, followed by C- and then the B-models (Figure 5a). This correlates with the value of the granular temperature at the core (see Figure 5b).

The time-averaged gas turbulent kinetic energy is also plotted in Figure 5b for the B- and C- models (A-model is not plotted because it does not include a $k-\varepsilon$ model). The discontinuity in the values of k next to the walls is because of the wall function. The level of turbulent kinetic energy (k) in the core of the channel predicted by Cao and Ahmadi is substantially greater than that predicted by Balzer et al. The C-model predicts similar values of gas and solids fluctuating energy considering the different definitions of $k=\frac{1}{2}\langle u'_g u'_g\rangle$ and $\Theta_s=\frac{2}{3}\langle u'_s u'_s\rangle$. The B-model predicts much lower values of k as most of the turbulent energy in the gas phase is dissipated by the presence of solid particles. It is not clear which model is more accurate as particles are known not only to dampen gas turbulence but also to increase it because of wake induced turbulence.[29,40] Nevertheless, the magnitude and shape of gas turbulent kinetic energy profiles predicted by models B and C do not have a significant effect on the solids fraction distribution or the gas velocity profile (Figures 5a, c), quite unlike single-phase turbulent flows. The gas flow pattern in this case is governed by the clusters and streamers; animations (see http://www.mfix.org/results/1-D.avi) of the simulations show that when clusters form on one side of the channel, the gas flow adjusts to the other side. Furthermore, we'll show in the next section that the gas-phase turbulent shear stresses can be neglected in the simulations under the flow conditions used in this study.

Figure 5d shows that similar time-averaged solids velocity profiles are computed for all three models. However, the B-model predicts slightly higher solids velocity everywhere, especially at the core of the channel, apparently because it predicts the lowest solids viscosity (Figure 5e). In the annulus region the flow of solids is downward. This is because gas bypasses the clusters forming near the walls, allowing them to fall because of gravity.

The different values of granular temperature predicted at the core of the channel (Figure 5b) cannot be explained by differences in the turbulent energy interaction terms because all three models use the same sink term ($3\beta\Theta_s$), which is usually larger than the turbulence interaction production

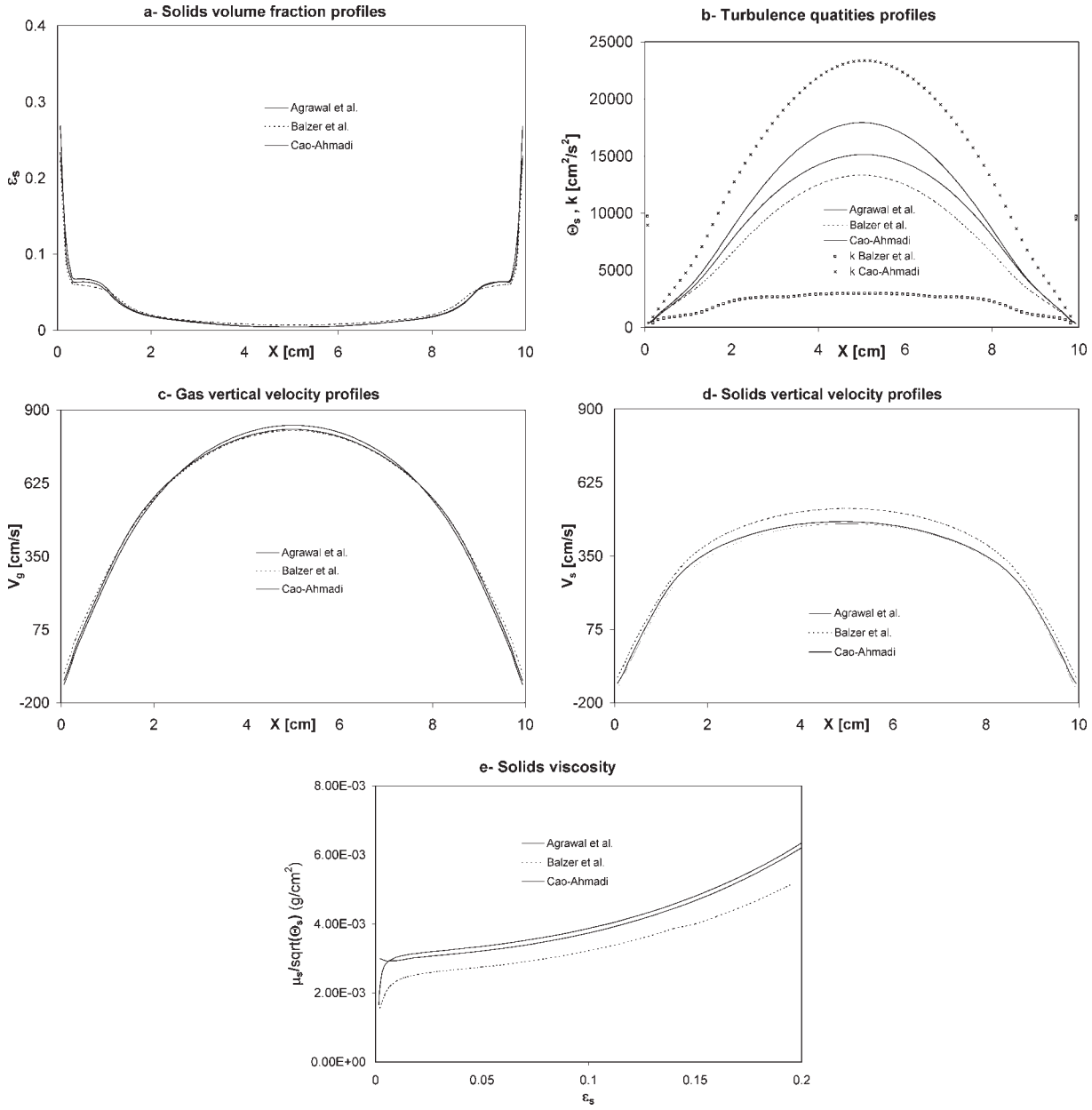

Figure 5. Effect of different gas/solids flow models (A, B and C; Agrawal et al.,[17] Balzer et al.,[16] and Cao-Ahmadi[15]) on the time-averaged flow variables (solids volume fraction, granular temperature and gas turbulent kinetic energy, and gas and solids velocities) plotted across the width of the channel.

Also plotted are the instantaneous solids viscosities (e) as a function of solids volume fraction for the three different models used in this study.

terms (as expressed in Eqs. A25–A28). So we look elsewhere for an explanation. Figure 5e shows the solids viscosity profiles normalized by $\sqrt{\Theta_s}$, to make the solids viscosity independent of granular temperature. For a given value of granular temperature, the highest solids viscosity is computed by the A-model followed by C- and B-models. Since the granular energy production rate is proportional to the shear rate and the solids viscosity, for a given shear rate the A-model will predict the highest granular temperature, which explains the ordering in Figure 5b.

The three gas/solids flow models considered in this study predict similar core-annulus flow regime, which suggest that using the KTGF is sufficient to model moderately dense flows such as the one considered here. Therefore, we choose the A-model for the rest of this study (except for the use of B-model for evaluating wall functions in next section), which simplifies the gas/solids flow model since the $k - \varepsilon$ equations are not included in this formalism.

Effect of BC on Core-Annulus Flow

The Johnson and Jackson[21] and Jenkins[22] BC are given in Table A3. The Jenkins BC shown here includes a modification[35] to ensure coordinate invariance, using the ratio of sol-

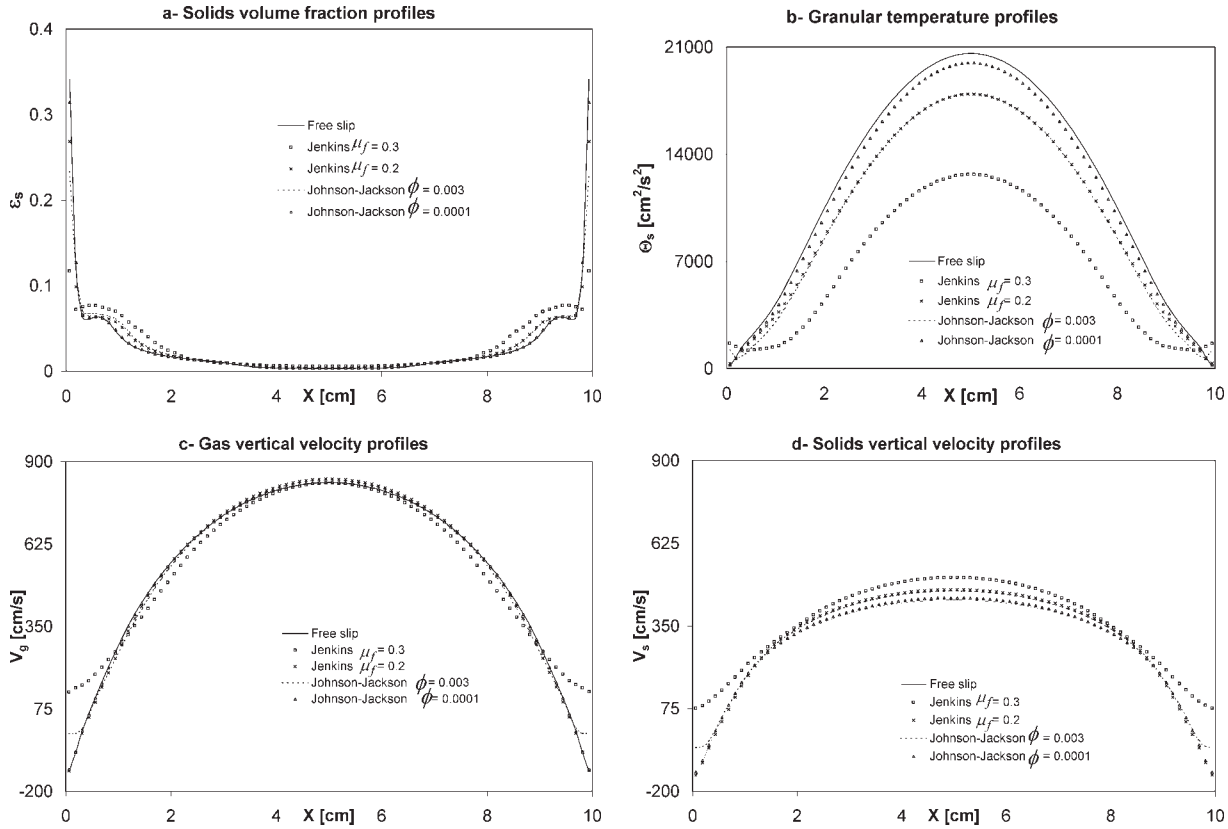

Figure 6. Effect of different boundary conditions for the solids phase (free slip, Jenkins—with two values of particle-wall friction coefficient—and Johnson and Jackson) on the time-averaged flow variables (solids volume fraction, granular temperature, and gas and solids velocities) across the channel.

ids velocity to the magnitude of the velocity (Eq. A32) The third BC studied is a free slip condition for solids velocity and a specified zero value for granular temperature at the walls.

Figure 6 shows various time-averaged profiles obtained using these three BC, for two parameter values in both the Jenkins and Johnson–Jackson BC. The BC has a more pronounced effect on the solids velocity profile than the turbulence models (compare Figure 6a with Figure 5a). The time-averaged solids concentration at the walls of the channel is the highest in the case of free slip BC, a counter-intuitive result to be explained later. A 50% increase (from 0.2 to 0.3) in the friction coefficient (μ_f) in Jenkins BC causes a 56% reduction in the solids volume fraction at the walls (from 0.27 to 0.12). Similarly, an increase in the value of the specularity coefficient in Johnson–Jackson BC, which is equivalent to an increase in particle-wall friction,[23,25] results in a reduction in the solids volume fraction at the walls. Animation of gas/solids flow patterns shows that the reduction in time-averaged solids volume fraction at walls is caused by the clusters tending to form away from the wall when the particle-wall friction is increased.

The BC represents the flux of energy into the granular medium at the walls. If the flux is positive then granular energy is produced at the wall. With the Jenkins BC, as the particle-wall friction increases, the minimum in the granular temperature profile is no longer at the wall, but a short distance away. This flux is positive when $\mu_f > \sqrt{(2/7)(1-e_w)/(1+e_w)}$. For $e_w = 0.7$, used in this study, the flux is positive when $\mu_f > 0.225$. Therefore, since granular energy is produced at the wall, the granular temperature increases there causing the solids to be pushed to the interior, destroying the core-annulus regime. A similar analysis of the Johnson and Jackson BC yields $\phi > (3(1-e_w^2)/2)(\Theta_s/u_s^2)$ for the flux to be positive. This limit on the specularity coefficient ϕ cannot be determined from material constants alone because the formula also depends on flow variables. Nevertheless, it has been observed in the calculations that even for values of ϕ as small as 0.003 granular energy gets produced at the walls. Very small values of ϕ (such as the value of 0.0001 used in this study) are necessary to prevent the production of granular energy at the wall, destabilizing the core-annulus regime. At such values of ϕ this BC is close to a free slip condition.

Figure 6b shows that the predicted granular temperature at the core decreases with increasing particle-wall friction for both the Jenkins and Johnson and Jackson BC. The free slip BC gives the highest granular temperature at the core. Therefore, it is clear that solids-wall friction is not the dominant production mechanism of granular energy in the solids phase. The production of granular energy is mainly due to gradients in the solids velocity. The highest gradients near the walls are observed for the case of free slip or low frictional BC, as shown in Figure 6d. This is because higher solids concentrations were computed for the cases of lowest particle-wall friction (see Figure 6a).

Figure 6c shows that gas flow at the core of the channel is not significantly affected by the solids phase BC, although

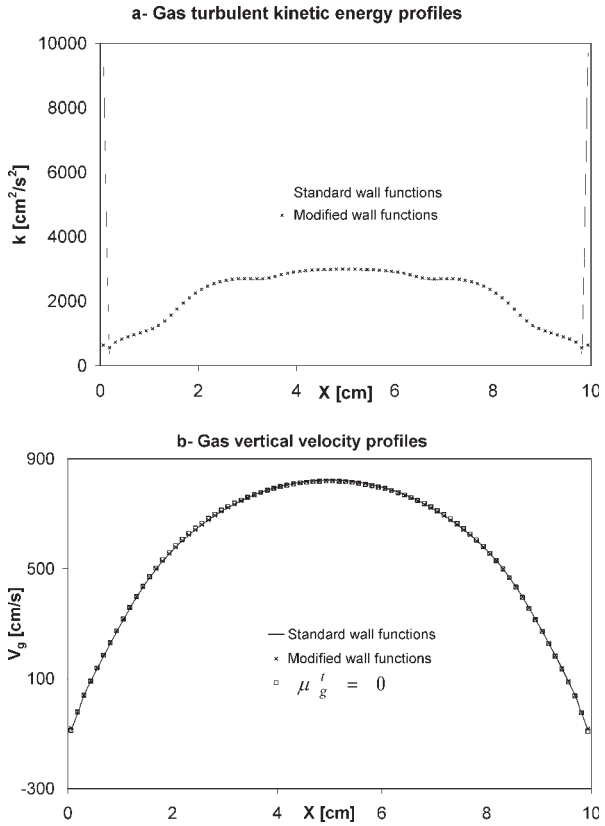

Figure 7. Time-averaged gas turbulent kinetic energy and velocity profiles across the channel using standard and modified (see Table A3) wall functions.

near the wall the gas flow closely follows the solids flow. Figure 7 shows the time-averaged profiles of gas turbulent kinetic energy and vertical gas velocity, using both standard and modified wall functions (Table A3) with B-model. Figure 7a shows a large difference between the standard and modified wall functions in the computed turbulent kinetic energy in the fluid cell next to the walls where these BC are applied. The modified wall function removes a discontinuity in the value of k near the wall calculated by the standard wall function. Everywhere else the standard and modified wall functions give nearly identical values of k. However, Figure 7b shows that this variation of the wall functions have no significant effect on the gas velocity profile. Obviously, there was no change in the solids velocity and granular temperature. Therefore, we conclude that the wall BC for the gas phase is not of importance in gas/solids flows of the type studied here. In very dilute flows, this may not be the case; for such calculations this modification to the wall function will probably be important. Using model B, we found that the average computed value of turbulent viscosity was about 44 times higher than the laminar viscosity. In spite of this fact, Figure 7b shows the same velocity profiles are obtained when the gas turbulent viscosity is set to zero in the gas momentum equations. Thus, the effects of the gas turbulent shear stresses can be neglected in these simulations.

This study shows that core-annulus flow can be predicted with low-frictional BC. This agrees with the argument[28] that the correct BC for the solids phase is a partial slip that is not far from free slip. For most cases in this study we have used the Jenkins low friction BC ($\mu_f = 0.2$). Similar results can be obtained using the Johnson and Jackson BC with very low specularity coefficient or, simply, a free slip BC. Modifications to wall functions had only minor effects on the predicted time-averaged results.

Effect of Particle–Particle Restitution Coefficient

Figure 8 shows the time-averaged predictions of the A-model for three values of the particle–particle restitution coefficient ($e = 0.9$, 0.99 and 0.999). For all three values, a core-annulus flow is predicted. Figure 8a shows that as e is increased, the time-averaged solids concentration at the walls decreases. This result is just the opposite of the conclusions based on steady state calculations, i.e., a large value of e ($e = 1$) is necessary to produce large solids concentration at the wall.[8,9] Figure 8b shows that as e increases, the granular temperature decreases everywhere. This is again counter to the intuitive conclusion that increasing the value of e decreases the dissipation of granular energy, thereby increasing the average granular temperature. This phenomenon has not been reported in the literature and only indirect evidence can be cited—a computational study,[41] based on the discrete particle method, showed that dissipation caused by inelastic collisions produced large inhomogeneities (or bubbles) in a fluidized bed. An earlier study by the same authors[42] showed that in a system with large inhomogeneities, indicating "intense particle collisions," large values of granular temperature were obtained. This indirectly shows that a decrease in restitution coefficient can increase the value of granular temperature in a bubbling bed because of the large-scale motion of bubbles that induce large gradients in the solids velocity.

The reduction in the average value of the granular temperature affects the gas and solids velocity profiles (Figures 8c, d). As the average granular temperature decreases, the solids viscosity values decrease, which leads to an increase in the average solids velocity. Recall that in these simulations only the average gas mass flux and solids volume fraction are fixed; the average solids mass flux is allowed to vary. So as the value of e increases so does the average solids velocity. Concurrently, the clusters near the wall become less dense (see Figure 9) and the downward solids velocity becomes smaller. This leads to smaller downward gas velocities near the wall. This is compensated for by smaller gas velocities at the core because the average gas mass flux is fixed. So as the value of e is increased the gas velocity at the core decreases in contrast to the solids velocity. Furthermore, because the solids concentration in the clusters decreases with increasing values of e as shown in Figure 9, the slip velocity between the gas and solids phases decreases as well.

Figure 8e, showing the solids mass flux profiles, reveals that the time-averaged values near the wall are negative for all three values of the restitution coefficient, although its magnitude decreases with increasing values of e. Contrast this with Figure 8d, which shows positive values of solids velocity near the wall for the two higher values of e. This is because the time-averaged solids mass flux ($\overline{\rho_s \varepsilon_s u_s}$) need not be equal to the time-averaged solids density multiplied by the time-averaged solids velocity ($\overline{\rho_s \varepsilon_s}\ \overline{u_s}$). The maximum solids mass flux is neither at

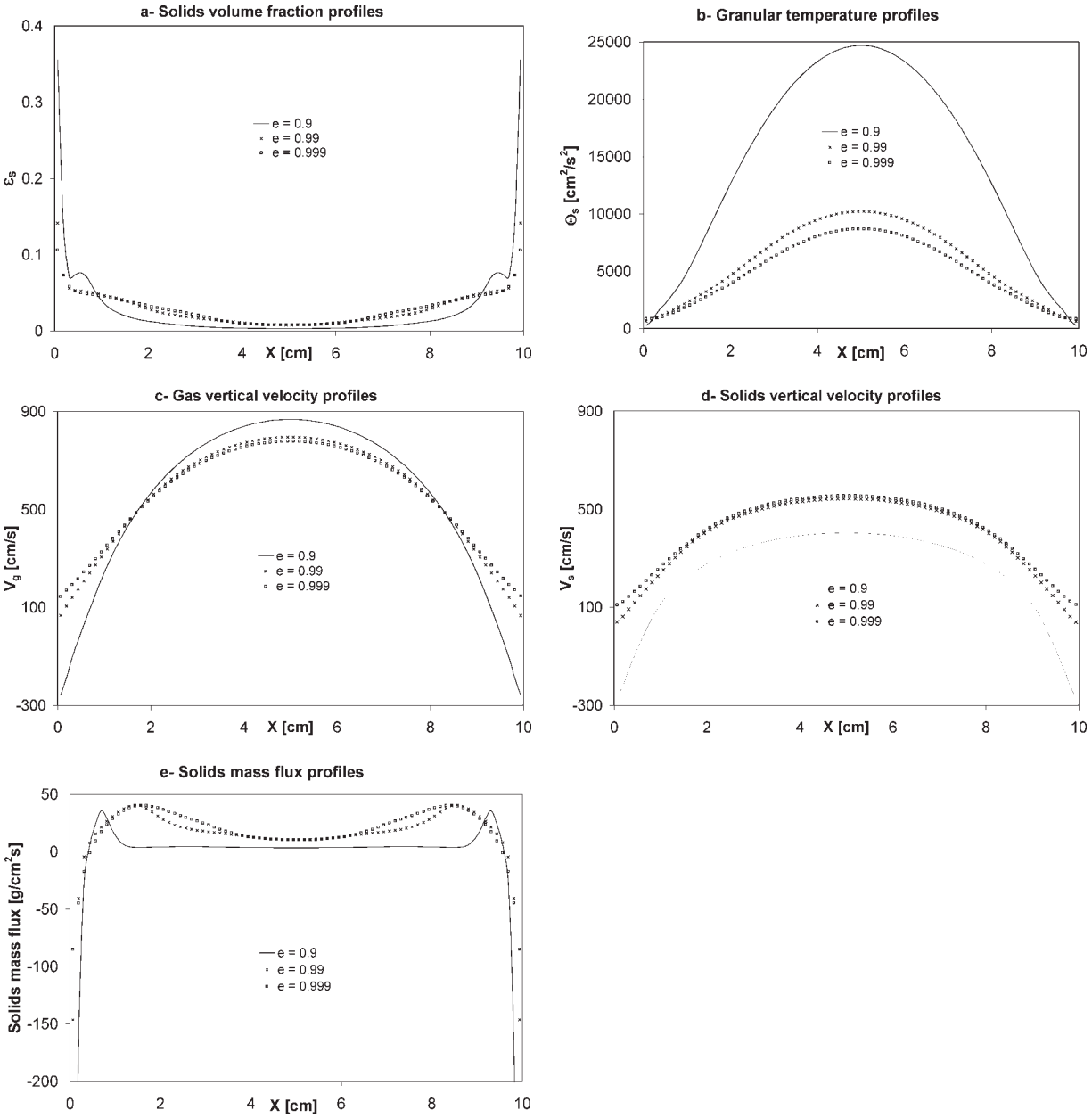

Figure 8. Effect of different values of the particle–particle restitution coefficient (*e*) on flow variables (solids volume fraction, granular temperature, gas and solids vertical velocities, and solids mass flux) profiles across the width of the channel, using the Agrawal et al. (A-) model.

the wall nor at the center, unlike the solids volume fraction or the velocity, but at a small distance away from the wall, which increases with the value of *e*. This could be a peculiarity of the 1D simulation because of the restricted degrees of freedom for particle recirculation; the predicted downward mass flux of solids at the walls is probably excessive. Preliminary results presented by the authors[38] showed that in 2D simulations the downward mass flux near the wall is smaller and the location of the maximum solids flux is closer to the center of the channel (see also Appendix B).

Figure 10 shows the time-averaged profiles of major dissipation and production terms in the granular energy equation. At the core of the channel, the low dissipation due to inelastic collisions (Figure 10a) and high production due to shear (Figure 10c) cause a high granular temperature (Figure 8b) and, consequently, a low solids concentration (Figure 8a). Adding the production and the dissipation terms (due to drag and inelastic collisions) results in a net production at the core of the channel. Figure 10a shows that the highest dissipation of granular energy was computed for the lowest value of $e = 0.9$. Figure 8a can be explained using simple physical arguments that the granular energy dissipation is a function of the square of solids volume fraction; hence more dissipation occurs at dense regions, which create cooler regions. Because of solids pressure, solids will migrate from hot regions (dilute) to dense flow regions (cool) as explained by

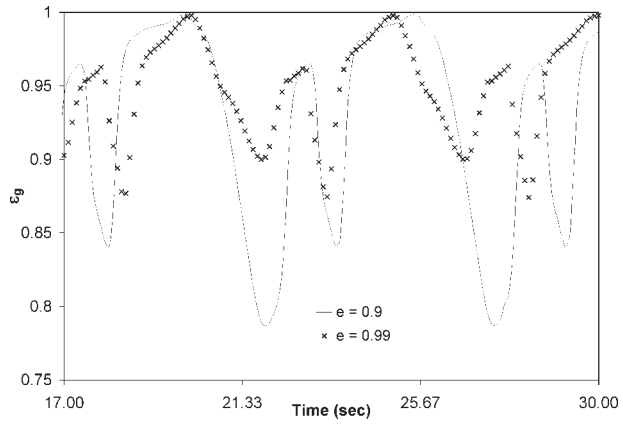

Figure 9. Transient profiles of gas volume fraction for two values of particle restitution coefficients (*e*) at a distance from the wall of about 0.56 cm; the clusters accumulating near the walls are denser for low values of *e*.

Goldhirsch et al.[43] This causes dense regions to get denser and dilute regions to be even more depleted of solids. Thus as the granular energy dissipation increases due to a decrease in e, we find it logical that clusters will get even denser (see Figure 9), and since we have a fixed solids concentration (3%) in this system, the dilute regions will have less solids because of mass conservation. Figure 9 shows transient profiles of gas volume fraction near the wall and demonstrate that denser clusters are computed for lower values of restitution coefficient. We'd like to point out again that "clusters" are dense flow regions that are transient because of their motion from one side wall to the other. Figure 10c shows that the highest production of granular energy was obtained for the lowest values of e. This explains the counter-intuitive result we saw earlier that the average granular temperature increases with decreasing values of e (Figure 8b). Much of the production due to shear occurs near the walls, associated with the down flow of clusters that occasionally form near the walls (see Figure 9). These clusters become denser as the value of e is decreased (as shown in Figure 9) because of the "cooling" effect[43] and the fact that denser clusters experience less drag and flow downward with increased velocity. Also, Figure 10c shows that the maximum production of granular energy was not exactly at the walls, but close to the walls. Furthermore, Figure 10c shows a high production due to shear $\left(\mu_s \frac{\partial V_s}{\partial X}\frac{\partial V_s}{\partial X}\right)$ at the center of the channel although the time-average velocity gradient $\overline{\frac{\partial V_s}{\partial X}}$ is zero at the center. This is because the time-averaged of the product of velocity gradients $\left(\overline{\frac{\partial V_s}{\partial X}\frac{\partial V_s}{\partial X}}\right)$ is not equal to the product of the time-averaged gradients $\left(\overline{\frac{\partial V_s}{\partial X}}\,\overline{\frac{\partial V_s}{\partial X}}\right)$. Therefore, any time-averaged governing equations must not neglect correlating the shear production because it is not possible to predict zero dissipation at the center of the channel for a particle restitution coefficient less than unity. This observation is fundamental for predicting a core-annulus flow because as mentioned earlier that this flow regime cannot be predicted unless the maximum granular temperature is computed at the center of the channel. Figure 10b shows that the maximum dissipation due to drag ($3\beta\Theta_s$) occurs at the center of the channel where granular temperature and slip velocity are the highest. Since clusters concentrate in regions of low granular energy, as explained by Goldhirsch et al.,[43] it is clear from Figure 10a that the formation of core-annulus flow is promoted by the dissipation due to inelastic collisions.

Steady State Results

We saw that the major mechanism for the production of granular energy is the shear generated by the transient dense

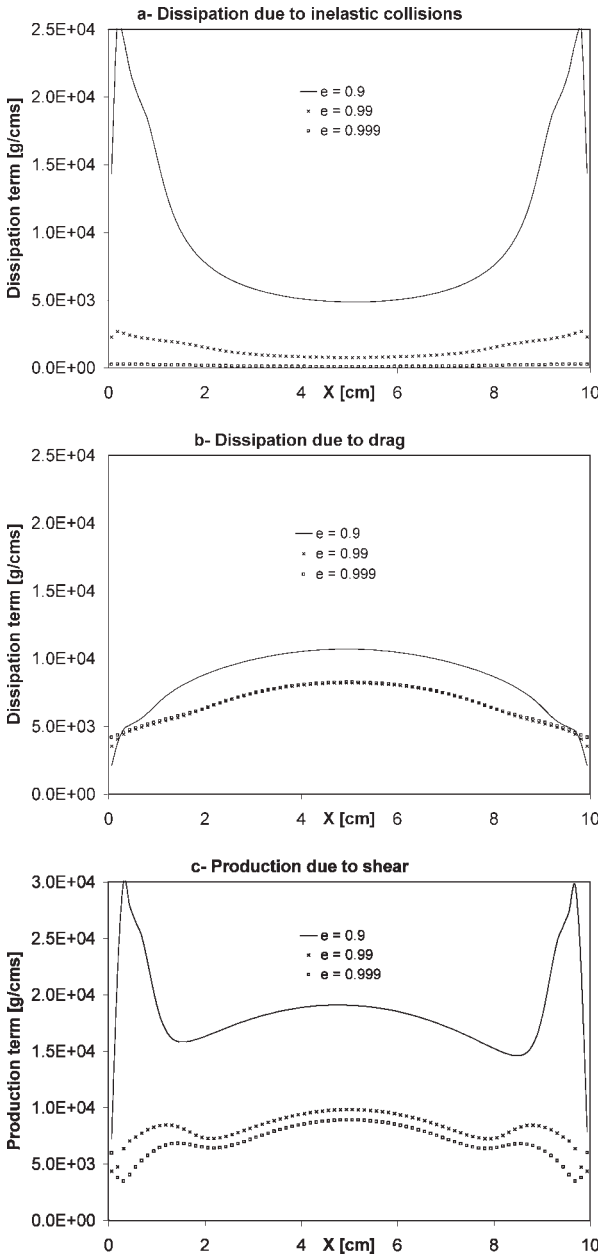

Figure 10. Time-averaged profiles of the major dissipation (inelastic particle–particle collisions and interphase exchange) and production (shear) terms in the granular temperature transport equation, which explain the granular temperature distribution in Figure 7b because of higher production at the center of the channel.

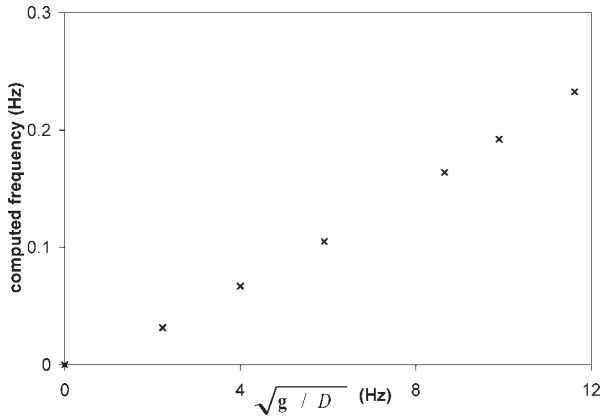

Figure 11. Verification of the scaling of oscillations frequency with the square root of the gravitational acceleration.

clusters forming near the walls and falling under the effect of gravity. We verify this observation by varying the gravitational acceleration using the values: 13.5, 9.8, 7.5, 3.5, 1.6 and 0 m/s^2. Figure 11 shows that the computed frequencies of oscillation scale linearly with the square root of gravity as determined by Gidaspow.[44] At zero gravity, a steady state was obtained and thus, a zero frequency was utilized in the plot. The length scale D used in $\sqrt{g/D}$ is the width of the riser. Under zero gravity, we found that a core-annulus flow was only computed by setting the dissipation terms to zero in the granular energy equation similar to previous studies using steady state models.[7–9] Otherwise, the computed steady state results show the highest concentration of solids at the center of the channel.

We further demonstrate the significant role played by the dissipation term in the granular energy equation—turning it off leads to a steady state solution even under Earth gravity. We used model A with no dissipation in the granular energy equation by setting e to unity and the exchange term to zero in Eq. A25. Furthermore, β is set to zero in the definition of granular viscosity and conductivity (Eqs. A15 and A21) so that model A resembles the model proposed by Lun et al.,[45] which is also mentioned as a "dry" granular model in the literature. The steady state solutions using this model required a high value of specularity coefficient since lower values produced much lower solids concentration near the wall, which is just the opposite of what we observed in transient simulations. This explains why researchers using steady-state models to compute core-annulus regime used high values of ϕ (a value of $\phi = 0.5$ was used in the literature[7,8,26]) whereas researchers using transient models use low values of ϕ (a value of $\phi = 0.01$ in Benyahia et al.[24]) or equivalently the free slip condition.[23,28] Therefore, we use a value of $\phi = 0.5$ in the remainder of this study. A reviewer pointed out that not all steady-state calculations use high values of ϕ as for example in the study of Bolio et al.[46] However that study was conducted for very dilute flow conditions, which does not fall within the core-annulus flow regime. Benyahia et al.[27] have computed a steady-state flow, using a transient model, for low solids loadings because the granular energy dissipation is negligible in these flow regimes because of its dependency on ε_s^2. A low value of ϕ was required to obtain reasonable agreement with experimental data for dilute flows.[27] In this study, we demonstrated that low values of ϕ are also required to obtain the experimentally observed core-annulus flow regime. In steady-state models that ignore the terms that arise from time-averaging use high values of ϕ because all the granular energy is produced by wall friction and not due to clusters motion as explained in this study.

Figure 12 shows the computed flow variables with no dissipation in the granular energy equation under Earth gravity and zero gravity. It is remarkable that the effect of gravity gets substantially diminished when the dissipation terms are turned off. This may have led Liu and Glasser[26] to comment about the "insensitivity to the magnitude of gravity," which at first looks counter to the conventional wisdom about fluidization that gravity is the most important force. The granular temperature profiles (Figure 12b) computed at the core of the channel are similar under both Earth gravity and zero gravity in spite of the differences in solids velocity profiles (see Figure 12d). This is because the solids velocity gradients, the only cause of granular energy production, are the same everywhere except near the walls. Therefore, there are differences in the granular temperature (Figure 12b) and the solids volume fraction (Figure 12a) only near the wall. The slip velocity is reduced when the gravitational acceleration is reduced (Figures 12c, d) Note that Liu and Glasser[26] computed the same slip velocity under different gravitational fields, mainly because of the different flow conditions used in their study: They fixed the solids flow rate, whereas in this study the averaged solids volume fraction or hold-up was fixed. Figure 12e shows the solids mass flux computed under Earth and zero gravity. The flow of solids is always upward even under Earth gravity. Removing the dissipation terms in the granular energy equation resulted in lower concentration of solids near the walls, which, in turn, caused positive solids mass flux near the walls of the channel.

Conclusions

In this study we evaluated frequently used continuum gas–solids models, BC and model parameters by conducting transient simulations of a 1D channel with a fixed average gas velocity of 5.5 m/s and solids volume fraction of 0.03. We used the condition that they be able to simulate the experimentally well-established core-annulus flow regime (high solids volume fraction at the walls and low at the center) as a sine quo non benchmark for the evaluation.

The number of computational cells required for ensuring the grid-independence of the solutions was determined for several discretization schemes. The second order scheme Superbee was found to give a grid-independent solution with a fewer number of computational cells, which was computationally faster than the first order upwind scheme. A cell size of about 10 particle diameters was necessary to achieve a grid-independent solution. We show that a coarse-grid solution, which is not grid-independent, is even qualitatively incorrect, showing large values of granular temperature with a maximum away from the core.

The three different gas/solids turbulence models evaluated in this study show very little effect on the predicted core-annulus flow regime. The gas turbulent shear stresses can be neglected for the moderately dense flow used in this study. The small variations between these models in the granular temperature and the solids velocity arose mainly because of variations in

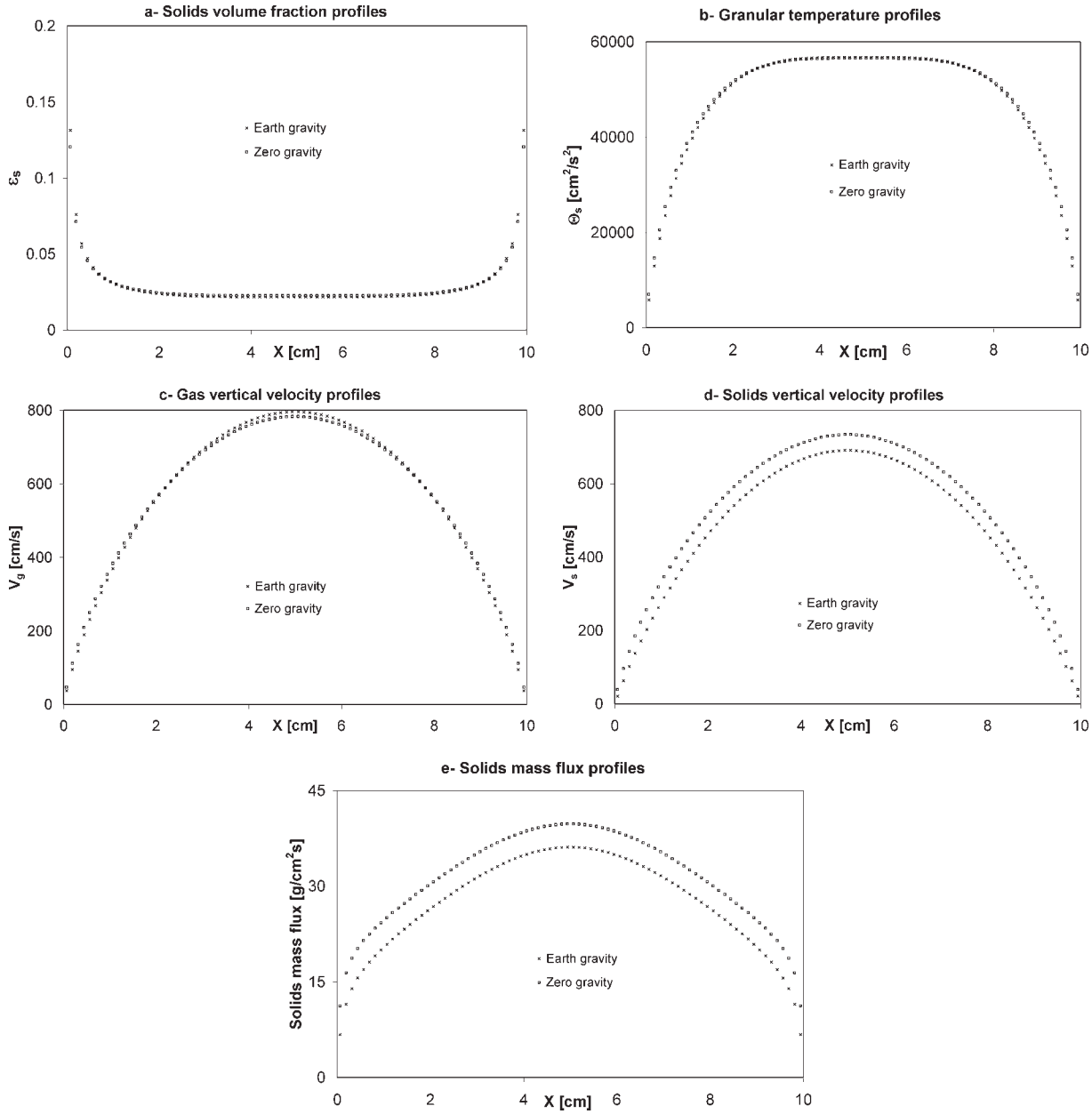

Figure 12. Comparison between steady-state results obtained under Earth gravity and zero gravity using the same model and boundary condition parameters.

The steady-state was achieved by assuming zero dissipation in the granular temperature equation or zero gravity.

the expressions for the solids viscosity. This suggests that KTGF is sufficient to model core-annulus flow regime.

Three wall BC for the solids phase were examined: Johnson and Jackson,[21] Jenkins,[22] and free slip with zero granular temperature at the wall. The free slip BC led to the highest solids concentration at the walls. The higher the particle-wall friction (higher values of the specularity coefficient in the Johnson and Jackson BC or higher values of the friction coefficient in the Jenkins BC) the lower is the solids concentration at the walls. A low friction at the wall is essential for producing a core-annulus flow regime.

Different BC for the gas phase (no-slip and free slip with the Agrawal et al.[17] model; standard and modified[27] wall functions with Balzer et al.[16] model) had negligible effect on the gas/solids flow patterns.

The model predictions are sensitive to the particle–particle restitution coefficient, but not unduly sensitive as in the case of steady state calculations. The main mechanism for production of granular energy is the shear caused by the clusters falling under gravity near the walls. As the restitution coefficient is decreased the solids concentration near the walls increases, inducing shear, and, consequently, the average granular temperature increases, a counter-intuitive result.

The inelasticity of particle–particle collisions causes a drop in the local granular temperature and, hence, granular

pressure. Thus, the transient solids concentration near the wall increases and induces a downward flow. That causes an increase in shear, which in turn causes the granular temperature to increase. This pushes material from the wall and reinitiates the cluster formation cycle. The core-annulus flow structure arises from the time averaging of such fluctuating motion.

The fluctuations are most sensitive to the gravitational acceleration term in the momentum equations and the dissipation term in the granular energy equation. Set either one of them to zero and the model predicts a steady state. The frequency of oscillations is proportional to the square root of the gravitational acceleration. Dissipation in the granular energy equation is the major mechanism that renders the flow unsteady and leads to cluster formation, the effect of which cannot be predicted with a steady model (without accounting for terms that arise from time-smoothing).

Notation

C_D = drag coefficient
C_μ, $C_{1\varepsilon}$, $C_{2\varepsilon}$, $C_{3\varepsilon}$ = constants in the gas turbulence model of values: 0.09, 1.44, 1.92, and 1.22, respectively
d_p = particle diameter
e = particle-particle restitution coefficient
e_w = particle-wall restitution coefficient
E = constant in wall function formulation equal to 9.81
g_i = acceleration of gravity in the i direction
g_0 = radial distribution function at contact
I_{nm} = momentum exchange
J_s = granular energy dissipation due to inelastic collisions
k = gas phase turbulent kinetic energy
k_{12} = cross-correlation of gas and solids fluctuating velocities in Balzer et al. model
P_m = pressure of phase m
S_{mij} = mean strain-rate tensor
U_m = averaged velocity of phase m

Greek letters

α = constant in the Agrawal et al. model equal to 1.6
β, β_{gs} = gas/solids friction coefficient
Δx = width of computational cell next to the wall
ε = turbulent energy dissipation in the gas phase
ε_m = volume fraction of phase m
ϕ = specularity coefficient
ζ_c, $\overline{\omega}_c$, and σ_c = constants depending on particle restitution coefficient
η = constant depending on particle restitution coefficient equal to $(1 + e)/2$
η_t = ratio between Lagrangian and particle relaxation time scales
κ = solids phase dilute granular conductivity
κ_v = von Karmen constant of value: 0.42
κ_s = conductivity of solids granular energy
μ = solids phase dilute granular viscosity
μ_b = bulk viscosity of the solids phase
μ_f = friction coefficient used in Jenkins BC
μ_g^e = effective gas turbulent viscosity
μ_g^t = turbulent eddy viscosity for gas phase
Π = turbulence exchange terms between gas and solids phases
ω_c = constant depending on particle restitution coefficient
θ = angle between mean particle velocity and mean relative velocity
Θ_s = granular temperature
ρ_m = density of phase m
σ_k, σ_ε = constants in the gas turbulence model of values: 1.0, 1.3, respectively
τ_{mij} = stress tensor of phase m
τ_{12}^x = particle relaxation time scale
τ_{12}^t = Eddy-particle interaction time scale
τ_1^t = energetic turbulent eddies time scale

Indices

g = gas phase
i, j = indices used to represent spatial direction and in Einstein summation convention
m = phase m: g for gas and s for solids phases
max = maximum packing
s, p = solids or particulate phase

Literature Cited

1. Gajdos LJ, Bierl TW. *Studies in support of recirculating fluidized bed reactors for the processing of coal*, Contract Topical Report DOE/EX-C-76-01-2449. Pittsburgh, PA: Carnegie Mellon University, 1976.
2. Weinstein H, Shao M, Schnitzlein M. Radial variation in solid density in high velocity fluidization. In: Basu P, editor. *Circulating Fluidized Bed Technology*. Elmsford, NY: Pergamon, 1986:201.
3. Bader R, Findlay J, Knowlton T. Gas/solid flow patterns in a 30.5-cm diameter circulating fluidized bed. In: Basu P, Large JF, editors. *Circulating Fluidized Bed Technology*, Vol. II. Elmsford, NY: Pergamon, 1988:123–137.
4. Miller A, Gidaspow D. Dense, vertical gas-solid flow in a pipe. *AIChE J*. 1992;38:1801–1815.
5. Bhusarapu S, Al-Dahhan MH, Duduković MP. Solids flow mapping in a gas–solid riser: mean holdup and velocity fields. *Powder Technol*. 2006;163:98–123.
6. Karri SBR, Knowlton TM. Flow direction and size segregation of annulus solids in a riser. In: Fan LS, Knowlton TM, editor. *Fluidization* IX. 1998:189–196.
7. Sinclair JL, Jackson R. Gas-particle flow in a vertical pipe with particle-particle interactions. *AIChE J*. 1989;35:1473–1486.
8. Pita JA, Sundaresan S. Gas-solid flow in vertical tubes. *AIChE J*. 1991;37:1009–1018.
9. Yasuna JA, Moyer HR, Elliott S, Sinclair JL. Quantitative predictions of gas-particle flow in a vertical pipe with particle-particle interactions. *Powder Technol*. 1995;84:23–34.
10. Foerster SF, Louge MY, Chang H, Allia K. Measurements of the collision properties of small spheres. *Phys Fluids*. 1995;6:1108–1115.
11. Brilliantov NV, Pöschel T. *Kinetic Theory of Granular Gases*. Oxford: Oxford University Press, 2004.
12. Shaffer F, Massah H, Sinclair J, Shahnam M.Measurement of time-averaged particle-wall collision properties using particle tracking velocimetry. *CRADA PC93–006, Final Report, DOE/FETC-99/1088*. Springfield, VA: National Technical Information Service.
13. Tsuo YP, Gidaspow D. Computation of flow patterns in circulating fluidized beds. *AIChE J*. 1990;36:885–896.
14. Ding J, Gidaspow D. A bubbling fluidization model using kinetic theory of granular flow. *AIChE J*. 1990;36:523–538.
15. Cao J, Ahmadi G. Gas-particle two-phase turbulent flow in a vertical duct. *Int J Multiphase Flow*. 1995;21:1203–1228.
16. Balzer G, Simonin O, Boelle A, Lavieville J. A unifying modelling approach for the numerical prediction of dilute and dense gas-solid two phase flow. In: *CFB5, 5th International Conference on Circulating Fluidized Beds*, Beijing, China, 1996.
17. Agrawal K, Loezos PN, Syamlal M, Sundaresan S. The role of meso-scale structures in rapid gas-solid flows, *J Fluid Mech*. 2001;445:151–185.
18. Dasgupta S, Jackson R, Sundaresan S. Turbulent gas-particle flow in vertical risers. *AIChE J*. 199440;215–228.
19. Hrenya CM, Sinclair JL. Effects of particulate-phase turbulence in gas-solids flows. *AIChE J*. 1997;42:853–869.
20. Curtis JS, van Wachem B. Modeling particle-laden flows: a research outlook. *AIChE J*. 2004;50:2638–2645.
21. Johnson PC, Jackson R. Frictional-collisional constitutive relations for granular materials, with application to plane shearing. *J Fluid Mech*. 1987;176:67–93.
22. Jenkins JT. Boundary conditions for rapid granular flow: flat, frictional walls. *Trans ASME*. 1992;59:120–127.

23. Neri A, Gidaspow D. Riser hydrodynamics: simulation using kinetic theory. *AIChE J*. 2000;46:52–67.
24. Benyahia S, Arastoopour H, Knowlton TM, Massah H. Simulation of particles and gas flow behavior in the riser section of a circulating fluidized bed using the kinetic theory approach for the particulate phase. *Powder Technol*. 2000;112:24–33.
25. Jones NE. An experimental investigation of particle size distribution effect in dilute phase gas-solid flow, PhD Dissertation. West Lafayette, IN: Purdue University, 2001.
26. Liu X, Glasser BJ. A parametric investigation of gas-particle flow in a vertical duct. *AIChE J*. 2006;52:940–956.
27. Benyahia S, Syamlal M, O'Brien TJ. Evaluation of boundary conditions used to model dilute, turbulent gas/solids flows in a pipe. *Powder Technol*. 2005;156:62–72.
28. Andrews AT, Loezos PN, Sundaresan S. Coarse-grid simulation of gas-particle flows in vertical risers. *Ind Eng Chem Res*. 2005;44:6022–6037.
29. Bolio EJ, Sinclair JL. Gas turbulence modulation in the pneumatic conveying of massive particles in vertical tubes. *Int J Multiphase Flow*. 1995;21:985–1001.
30. De Wilde J, Marin GB, Heynderickx G. The effects of an abrupt T-outlet in a riser: 3D simulation using the kinetic theory of granular flow. *Chem Eng Sci*. 2003;58:877–885.
31. Gidaspow D. *Multiphase Flow and Fluidization: Continuum and Kinetic Theory Description*. San Diego: Academic Press, 1994.
32. Kandhai D, Derksen JJ, van den Akker, HEA. Interphase drag coefficients in gas-solid flows. *AIChE J*. 2003;49:1060–1065.
33. Srivastava A, Sundaresan S. Analysis of a frictional-kinetic model for gas-particle flow. *Powder Technol*. 2003;129:72–85.
34. van Wachem BGM, Schouten JC, Krishna R, van den Bleek CM. CFD modeling for gas-solid flows: qualitative and quantitative analysis of the various treatments. In: *Proceedings of the 3rd ASME/JSME Joint Fluids Engineering Conference*, San Francisco, CA, July 18–23, 1999.
35. Benyahia S, Syamlal M, O'Brien TJ. Summary of MFIX equations, Version 2005-4. 2006. Available at http://www.mfix.org/documentation/MfixEquations2005-4-1.pdf.
36. Syamlal M, Rogers W, O'Brien TJ. *MFIX documentation: theory guide*, Technical Note, DOE/METC-94/1004, NTIS/DE94000087. Springfield, VA: National Technical Information Service, 1993.
37. Syamlal M. *MFIX documentation: numerical techniques*, DOE/MC-31346–5824 NTIS/DE98002029. Springfield, VA: National Technical Information Service, 1998.
38. Benyahia S, Syamlal M, O'Brien TJ. Consistency of fully developed and periodic simulations in gas/solids flow in a riser. Presented at the AICHE Annual Meeting, Cincinnati, OH, 2005.
39. Guenther C, Syamlal M. The effect of numerical diffusion on simulation of isolated bubbles in a gas–solid fluidized bed. *Powder Technol*. 2001;116:142–154.
40. Sundaresan S, Eaton J, Koch D, Ottino JM. Appendix 2: report of study group on disperse flow. *Int J Multiphase Flow*. 2003;29:1069–1087.
41. Li J, Kuipers JAM. Gas-particle interactions in dense gas-fluidized beds. *Chem Eng Sci*. 2003;58:711–718.
42. Li J, Kuipers JAM. Effect of pressure on gas–solid flow behavior in dense gas-fluidized beds: a discrete particle simulation study. *Powder Technol*. 2002;127:173–184.
43. Goldhirsch I, Noskowicz SH, Bar-Lev O. Theory of granular gases: some recent results and some open problems. *J Phys: Condens Matter*. 2005;17:2591–2608.
44. Gidaspow D. Hydrodynamics of fluidization using kinetic theory: an emerging paradigm? *Recent Res Dev Chem Eng*. Trivandrum, India, Transworld Research Network. 2003;5:53–81.
45. Lun CKK, Savage SB, Jeffrey DJ, Chepurniy N. Kinetic theories of granular flows: inelastic particles in Couette flow and slightly inelastic particles in a general flow field. *J Fluid Mech*. 1984;140:223–256.
46. Bolio EJ, Yasuna JA, Sinclair JL. Dilute turbulent gas-solid flow in risers with particle-particle interactions. *AIChE J*. 1995;41:1375–1388.
47. Syamlal M, O'Brien TJ. Fluid dynamic simulation of O_3 decomposition in a bubbling fluidized bed. *AIChE J*. 2003;49:2793–2801.
48. Guenther C, Syamlal M, Shadle L, Ludlow C. A numerical investigation of an industrial scale gas-solids CFB. In: *Proceedings of the 7th International Conference on Circulating Fluidized Beds*, Niagara Falls, Ontario, Canada, May 5–8, 2002.

Appendix A

The gas/solids flow models used in this study are summarized in this appendix. Agrawal et al.[17] model was used in most of this study. It contains an adjustable parameter ($\alpha = 16$) that was determined empirically by Johnson and Jackson.[21] We have also used a granular model similar to that developed by Lun et al.[45] and can be obtained easily from the Agrawal et al. model by setting the phase-exchange term to zero in the granular temperature equation and the drag to zero in the solids viscosity and conductivity. The Balzer et al.[16] and Cao and Ahmadi[15] models include a modified $k-\varepsilon$ model that is not used by the Agrawal et al. Table A3 shows the BC for the solids and gas phases used in this study. The Jenkins[22] and Johnson and Jackson[21] BC were used for the solids phase. Benyahia et al.[27] used standard and modified wall functions that are also presented in Table A3.

Appendix B

We compare in this appendix results obtained in a 2D and 1D systems using the same model (model A) and BC (Jenkins BC). The results obtained in the 2D system were presented in an AIChE meeting,[38] but are not easily accessible as pointed out by a reviewer. The 2D system had a height to width ratio (L/D) equal to 4, which was found by Agrawal et al.[17] to be sufficient to resolve all the flow structures. A

Table A1. Governing Equations for Gas/Solids Flows

Mass conservation for phase m (m = g for gas and s for solids)

$$\frac{\partial}{\partial t}\left(\varepsilon_{\mathrm{m}}\rho_{\mathrm{m}}\right)+\frac{\partial}{\partial x_i}\left(\varepsilon_{\mathrm{m}}\rho_{\mathrm{m}}U_{\mathrm{m}i}\right)=0 \tag{A1}$$

Momentum conservation for phase m

$$\left[\frac{\partial}{\partial t}\left(\varepsilon_{\mathrm{m}}\rho_{\mathrm{m}}U_{\mathrm{m}i}\right)+\frac{\partial}{\partial x_j}\left(\varepsilon_{\mathrm{m}}\rho_{\mathrm{m}}U_{\mathrm{m}j}U_{\mathrm{m}i}\right)\right] = -\varepsilon_{\mathrm{m}}\frac{\partial P_{\mathrm{g}}}{\partial x_i}+\frac{\partial \tau_{\mathrm{m}ij}}{\partial x_j}-I_{\mathrm{nm}i}+\varepsilon_{\mathrm{m}}\rho_{\mathrm{m}}g_i \tag{A2}$$

Modified gas phase $k-\varepsilon$ turbulence model

$$\varepsilon_{\mathrm{g}}\rho_{\mathrm{g}}\left[\frac{\partial k}{\partial t}+U_{\mathrm{g}j}\frac{\partial k}{\partial x_j}\right]=\frac{\partial}{\partial x_i}\left(\varepsilon_{\mathrm{g}}\frac{\mu_{\mathrm{g}}^{t}}{\sigma_k}\frac{\partial k}{\partial x_i}\right)+\varepsilon_{\mathrm{g}}\tau_{\mathrm{g}ij}\frac{\partial U_{\mathrm{g}i}}{\partial x_j}+\Pi_k-\varepsilon_{\mathrm{g}}\rho_{\mathrm{g}}\varepsilon \tag{A3}$$

$$\varepsilon_{\mathrm{g}}\rho_{\mathrm{g}}\left[\frac{\partial \varepsilon}{\partial t}+U_{\mathrm{g}j}\frac{\partial \varepsilon}{\partial x_j}\right]=\frac{\partial}{\partial x_i}\left(\varepsilon_{\mathrm{g}}\frac{\mu_{\mathrm{g}}^{t}}{\sigma_\varepsilon}\frac{\partial \varepsilon}{\partial x_i}\right)+\varepsilon_{\mathrm{g}}\frac{\varepsilon}{k}\times\left(C_{1\varepsilon}\,\tau_{\mathrm{g}ij}\frac{\partial U_{\mathrm{g}i}}{\partial x_j}-\rho_{\mathrm{g}}C_{2\varepsilon}\varepsilon\right)+\Pi_\varepsilon \tag{A4}$$

Granular energy transport equation

$$\frac{3}{2}\varepsilon_{\mathrm{s}}\rho_{\mathrm{s}}\left[\frac{\partial \Theta_{\mathrm{s}}}{\partial t}+U_{\mathrm{s}j}\frac{\partial \Theta_{\mathrm{s}}}{\partial x_j}\right]=\frac{\partial}{\partial x_i}\left(\kappa_{\mathrm{s}}\frac{\partial \Theta_{\mathrm{s}}}{\partial x_i}\right)+\tau_{\mathrm{s}ij}\frac{\partial U_{\mathrm{s}i}}{\partial x_j}+\Pi_\Theta-\varepsilon_{\mathrm{s}}\rho_{\mathrm{s}}J_{\mathrm{s}} \tag{A5}$$

Table A2. Constitutive Relations for Gas/Solids Flows

Gas/solids momentum exchange term

$$I_{gsi} = \beta_{gs}\left(U_{gi} - U_{si}\right), \qquad \beta_{gs} = \frac{3}{4} C_D \frac{\rho_g \varepsilon_g \varepsilon_s \left|U_g - U_s\right|}{d_p} \varepsilon_g^{-2.65}$$
$$C_D = \begin{cases} 24/Re\left(1 + 0.15\, Re^{0.687}\right) & Re < 1000 \\ 0.44 & Re > 1000 \end{cases}, \; Re = \frac{\rho_g \varepsilon_g \left|U_g - U_s\right| d_p}{\mu_g} \tag{A6}$$

Gas phase stress term

$$\tau_{gij} = 2\mu_g^e S_{gij}, \qquad S_{gij} = \frac{1}{2}\left(\frac{\partial U_{gi}}{\partial x_j} + \frac{\partial U_{gj}}{\partial x_i}\right) - \frac{1}{3}\frac{\partial U_{gi}}{\partial x_i}\delta_{ij} \tag{A7}$$

Gas phase viscosity model

$$\mu_g^e = \min\left(\mu_{max}, \mu_g + \mu_g^t\right) \tag{A8}$$

For Balzer et al.: $\mu_g^t = \rho_g C_\mu \dfrac{k^2}{\varepsilon}$ (A9)

For Cao and Ahmadi: $\mu_g^t = \rho_g C_\mu \left[1 + \left(\tau_{12}^x/\tau_1^t\right)\left(\varepsilon_s/\varepsilon_s^{max}\right)^3\right]^{-1} \dfrac{k^2}{\varepsilon}$ (A10)

Solids phase stress term

$$\tau_{sij} = \left(-P_s + \eta\mu_b \frac{\partial U_{si}}{\partial x_i}\right)\delta_{ij} + 2\mu_s S_{sij}, \qquad S_{sij} = \frac{1}{2}\left(\frac{\partial U_{si}}{\partial x_j} + \frac{\partial U_{sj}}{\partial x_j}\right) - \frac{1}{3}\frac{\partial U_{si}}{\partial x_i} \tag{A11}$$

Solids pressure models

For Agrawal et al. or Balzer et al.: $P_s = \varepsilon_s \rho_s \Theta_s [1 + 4\eta\varepsilon_s g_0]$ (A12)

For Cao and Ahmadi: $P_s = \varepsilon_s \rho_s \Theta_s \left[1 + 4\varepsilon_s g_0 + 0.5\left(1 - e^2\right)\right]$ (A13)

Solids viscosity models

For Agrawal et al.: $\mu_s = \left(\dfrac{2+\alpha}{3}\right)\left[\dfrac{\mu_s^*}{g_0\eta(2-\eta)}\left(1 + \dfrac{8}{5}\eta\varepsilon_s g_0\right)\left(1 + \dfrac{8}{5}\eta(3\eta - 2)\varepsilon_s g_0\right) + \dfrac{3}{5}\eta\mu_b\right]$ (A14)

$$\mu_s^* = \frac{\rho_s \varepsilon_s g_0 \Theta_s \mu}{\rho_s \varepsilon_s g_0 \Theta_s + \left(\frac{2\beta\mu}{\rho_s \varepsilon_s}\right)}, \qquad \mu = \frac{5}{96}\rho_s d_p \sqrt{\pi\Theta_s}, \qquad \mu_b = \frac{256}{5\pi}\mu\varepsilon_s\varepsilon_s g_0 \tag{A15}$$

For Balzer et al.: $\mu_s = \varepsilon_s \rho_s \left\{\left[\dfrac{2}{3}k_{12}\eta_t + \Theta_s(1 + \zeta_{c2}\varepsilon_s g_0)\right]\left(1 + \dfrac{8}{5}\varepsilon_s g_0 \eta\right)\tau_2 + \dfrac{8}{5}\varepsilon_s g_0 \eta\, d_p \sqrt{\dfrac{\Theta_s}{\pi}}\right\}$ (A16)

$$\mu_b = \frac{8}{3}\varepsilon_s g_0 \eta\left[\left(\frac{2}{3}k_{12}\eta_t + \Theta_s(1 + \zeta_{c2}\varepsilon_s g_0)\right)\tau_2 + d_p\sqrt{\frac{\Theta_s}{\pi}}\right] \tag{A17}$$

For Cao and Ahmadi: $\mu_s = \left[1 + \left(\tau_1^t/\tau_{12}^x\right)\left(1 - \varepsilon_s/\varepsilon_s^{max}\right)^3\right]^{-1}\left[0.1045\left(1/g_0 + 3.2\varepsilon_s + 12.1824 g_0 \varepsilon_s^2\right) d_p \rho_s \sqrt{\Theta_s}\right]$ (A18)

$$\mu_b = \frac{5}{3}\left[1 + \left(\tau_1^t/\tau_{12}^x\right)\left(1 - \varepsilon_s/\varepsilon_s^{max}\right)^3\right]^{-1}\left[0.1045\left(12.1824 g_0 \varepsilon_s^2\right) d_p \rho_s \sqrt{\Theta_s}\right] \tag{A19}$$

Granular conductivity models

For Agrawal et al.: $\kappa_s = \left(\dfrac{\kappa_s^*}{g_0}\right)\left[\left(1 + \dfrac{12}{5}\eta\varepsilon_s g_0\right)\left(1 + \dfrac{12}{5}\eta^2(4\eta - 3)\varepsilon_s g_0\right) + \dfrac{64}{25\pi}(41 - 33\eta)\eta^2(\varepsilon_s g_0)^2\right]$ (A20)

Table A2. Constitutive Relations for Gas/Solids Flows (Continued)

$$\kappa_s^* = \frac{\rho_s \varepsilon_s g_0 \Theta_s \kappa}{\rho_s \varepsilon_s g_0 \Theta_s + \left(\frac{6\beta\kappa}{5\rho_s\varepsilon_s}\right)}, \qquad \kappa = \frac{75\rho_s d_p \sqrt{\pi\Theta_s}}{48\eta(41-33\eta)} \tag{A21}$$

For Balzer et al.:

$$\kappa_s = \varepsilon_s\rho_s\left\{\left(\frac{9}{10}k_{12}\eta_t + \frac{3}{2}\Theta_s(1+\varpi_c\varepsilon_s g_0)\right)\left(\frac{9/5}{\tau_{12}^x}+\frac{\xi_c}{\tau_2^c}\right)^{-1}\left(1+\frac{18}{5}\varepsilon_s g_0\eta\right) + 2\varepsilon_s g_0\eta\, d_p\sqrt{\frac{\Theta_s}{\pi}}\right\} \tag{A22}$$

For Cao and Ahmadi: $\kappa_s = \frac{5}{3}\left[1+\left(\tau_1^t/\tau_{12}^x\right)\left(1-\varepsilon_s/\varepsilon_s^{\max}\right)^3\right]^{-1} \quad \left[0.1045\left(12.1824 g_0\varepsilon_s^2\right)d_p\rho_s\sqrt{\Theta_s}\right]$ (A23)

Collisional dissipation of granular energy

$$J_s = \frac{48}{\sqrt{\pi}}\eta(1-\eta)\frac{\varepsilon_s g_0}{d_p}\Theta_s^{3/2} \tag{A24}$$

Turbulence interaction terms

For Agrawal et al.: $\Pi_\Theta = -3\beta\Theta_s + \frac{81\varepsilon_s\mu_g^2\left|U_g-U_s\right|^2}{g_0 d_p^3\rho_s\sqrt{\pi\Theta_s}}$ (A25)

For Balzer et al.: $\Pi_\Theta = \beta(k_{12}-3\Theta_s), \qquad \Pi_k = \beta(k_{12}-2k), \qquad \Pi_\varepsilon = C_{3\varepsilon}(\varepsilon/k)\Pi_k$ (A26)

$$k_{12} = \frac{\eta_t}{1+(1+X_{21})\eta_t}(2k+3X_{21}\Theta_s) \tag{A27}$$

For Cao and Ahmadi: $\Pi_\Theta = \beta\left(\frac{2k}{1+\tau_{12}^x/\tau_1}-3\Theta_s\right), \Pi_k = \beta(3\Theta_s-2k), \qquad \Pi_\varepsilon = 0$ (A28)

Time scales and constants definition

$$\tau_{12}^x = \frac{\varepsilon_s\rho_s}{\beta}, \qquad \tau_1^t = \frac{3}{2}C_\mu\frac{k}{\varepsilon}, \qquad \tau_{12}^t = \frac{\tau_1^t}{\sqrt{1+C_\beta\xi_r^2}}, \quad \eta_t = \frac{\tau_{12}^t}{\tau_{12}^x},$$
$$\tau_2^c = \frac{d_p}{6\varepsilon_s g_0\sqrt{16\Theta_s/\pi}}, \qquad \frac{1}{\tau_2} = \frac{2}{\tau_{12}^x}+\frac{\sigma_c}{\tau_2^c} \tag{A29}$$

Constants in $k-\varepsilon$ model : $\sigma_k, \sigma_\varepsilon, C_\mu, C_{1\varepsilon}, C_{2\varepsilon}, C_{3\varepsilon} = 10, 13, 009, 144, 192,$ and $122,$ respectively (A30)

Additional parameters used in turbulence models : $\xi_r^2 = \frac{3|u_g-u_s|^2}{2k}, \qquad C_\beta = 1.8-1.35\,\cos^2(\theta),$
$$\zeta_{c2} = 2/5(1+e)(3e-1), \quad \varpi_c = (1+e)^2(2e-1)/100,$$
$$\zeta_c = (1+e)(49-33e)/100, \qquad \sigma_c = (1+e)(3-e)/5,$$
$$X_{21} = \frac{\varepsilon_s\rho_s}{\varepsilon_g\rho_g}, \qquad \eta = \frac{1+e}{2}, \qquad \alpha = 1.6 \tag{A31}$$

Table A3. Wall Boundary Conditions

Jenkins small frictional limit boundary condition

$$\mu_s \frac{\partial u_s}{\partial x} = -P_s \mu_f \frac{u_s}{|u_s|} \tag{A32}$$

$$\kappa_s \frac{\partial \Theta_s}{\partial x} = P_s \sqrt{3\Theta_s} \frac{3}{8} \left[\frac{7}{2}(1+e_w)\mu_f^2 - (1-e_w) \right] \tag{A33}$$

Johnson and Jackson boundary condition

$$\mu_s \frac{\partial u_s}{\partial x} = -\frac{\phi \pi \rho_s \varepsilon_s g_0 \sqrt{\Theta_s}}{2\sqrt{3}\varepsilon_s^{\max}} u_s \tag{A34}$$

$$\kappa_s \frac{\partial \Theta_s}{\partial x} = \frac{\phi \pi u_s^2 \rho_s \varepsilon_s g_0 \sqrt{\Theta_s}}{2\sqrt{3}\varepsilon_s^{\max}} - \frac{\sqrt{3}\pi \rho_s \varepsilon_s g_0 \left(1-e_w^2\right)\sqrt{\Theta_s}}{4\varepsilon_s^{\max}} \Theta_s \tag{A35}$$

Wall functions for gas phase boundary condition
Standard wall functions:

$$\frac{\partial u_g}{\partial x} = -\frac{\rho_g \kappa_v C_\mu^{1/4} \sqrt{k}}{\left(\mu_g + \mu_g^t\right) \ln(E\, x^*)} u_g, \qquad x^* = \frac{\rho_g C_\mu^{1/4} \sqrt{k} \Delta x/2}{\mu_g} \tag{A36}$$

$$\frac{\partial k}{\partial x} = 0; \qquad \frac{\partial \varepsilon}{\partial x} = 0 \tag{A37}$$

The following sets the production and dissipation of k as well as a value for ε at the fluid cells adjacent to walls:

$$\text{production of } k = \varepsilon_g \tau_{gij} \frac{\partial u_{gi}}{\partial x_j} = \varepsilon_g \rho_g \sqrt{C_\mu} k \frac{u_g}{\Delta x/2\ \ln(E\, x^*)} \tag{A38}$$

$$\text{dissipation of } k = \varepsilon_g \rho_g \varepsilon \tag{A39}$$

$$\varepsilon = \frac{C_\mu^{3/4} k^{3/2}}{\kappa_v \Delta x/2} \tag{A40}$$

Modified wall functions (modifications made only to production and dissipation of k):

$$\text{production of } k = \varepsilon_g \tau_{gij} \frac{\partial u_{gi}}{\partial x_j} + \beta\, k_{12} = \varepsilon_g \rho_g \sqrt{C_\mu k} \frac{u_g}{\Delta x/2\ \ln(E\, x^*)} + \beta\, k_{12} \tag{A41}$$

$$\text{dissipation of } k = \varepsilon_g \rho_g \varepsilon + 2\beta\, k \tag{A42}$$

computational grid ratio of one was also used in the 2D simulation with 80 and 320 grids used along the width and height of the channel, respectively.

The time-averaged results presented in Figure B1 show that a core-annulus flow regime was predicted in both 1D and 2D computational domains. The 2D model predicted a higher solids concentration at the center of about 2% instead of about 0.4% predicted by the 1D model because of the fact that clusters formed not only at the walls but occasionally at the center of the channel for the 2D model. However, the large-scale oscillations of clusters from one side wall to the other are similar using both 1D and 2D models (see the animations of transient simulation results for 1D and 2D models located at: http://www.mfix.org/results/1-D.avi and http://www.mfix.org/results/2-D.avi). The 2D clusters that formed near the walls fall under gravity with a lower velocity because of higher gas/solids interaction due to drag. Thus, the time-averaged solids velocity near the wall was positive for the 2D simulation with lower gradients that produced less granular temperature in the 2D simulation as seen in Figure B1b. By comparing the gas and solids velocities in Figures B1c, d, we can deduce a higher dimensionless slip velocity (made dimensionless with a terminal velocity of about 0.7 m/s) of about 3.5 for the 1D case as compared with a value of 2 computed in the 2D case. The slip velocity computed in the 2D case is closer to values reported by Agrawal et al.[17] Figure B1 shows the high downflow of solids at the walls of the channel in 1D was reduced in 2D. The solids mass flux is much higher at the center of the channel for the 2D case because of higher solids concentration. Figure B2 shows a

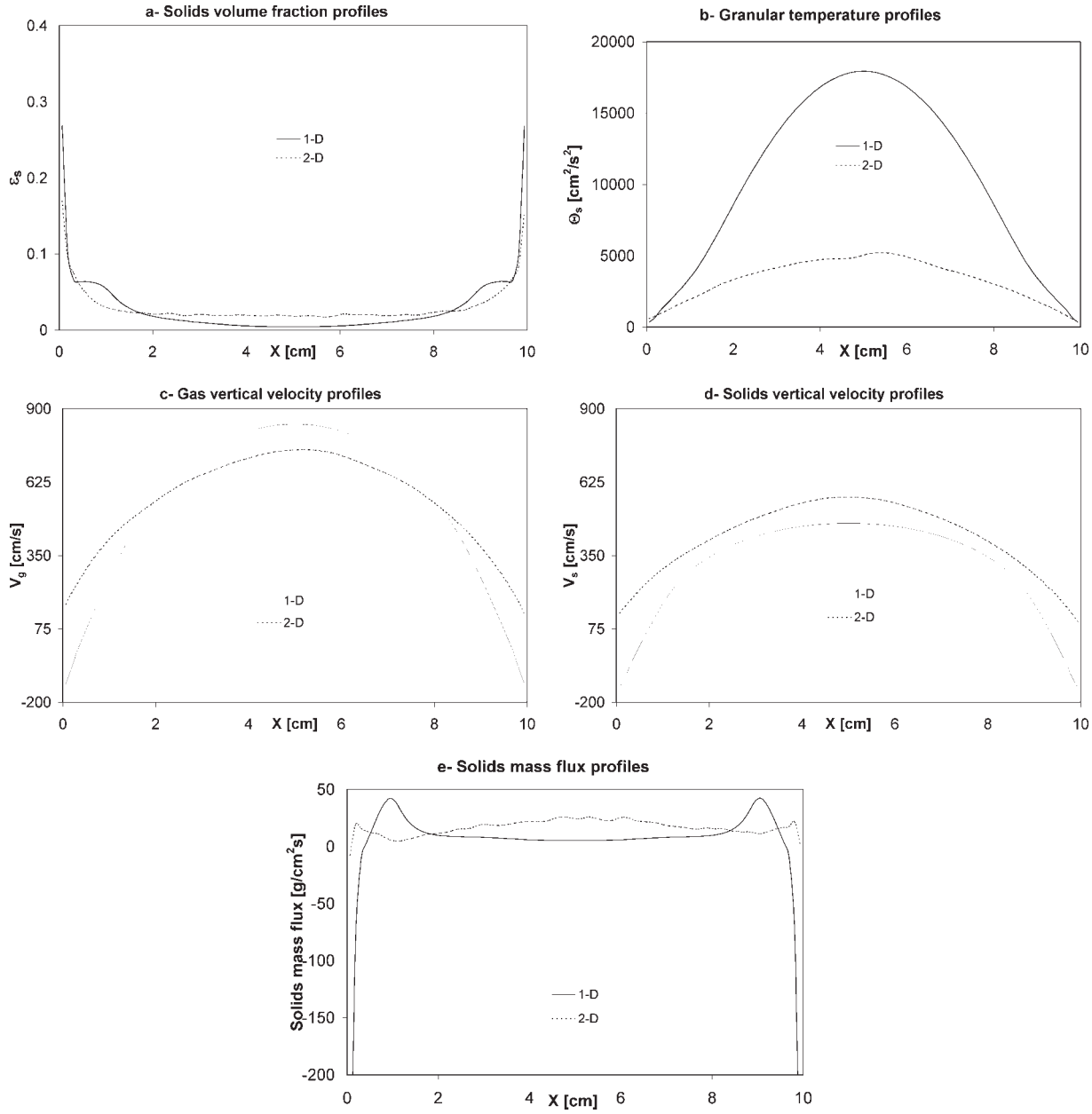

Figure B1. Comparison of time-averaged results obtained in 1D and 2D systems.

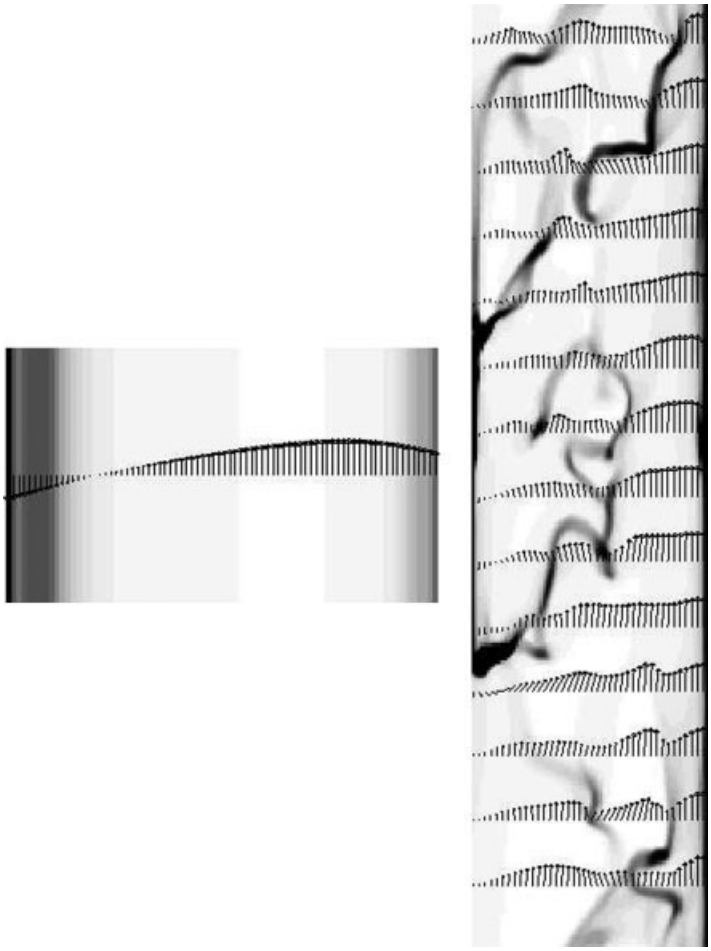

Figure B2. Instantaneous grayscale plots of solids volume fractions and gas velocity vectors in 1D and 2D systems.

A maximum of 20% solids volume fraction indicated with black color show clusters and strands in the 2D system and stripes in 1D. Dilute regions are indicated with white color.

snapshot of solids volume fraction distribution in the 1D and 2D channels. The strips of highly concentrated solids computed in the 1D simulation are different from the 2D clusters and strands predicted by the 2D simulation. The 2D clusters are visible not only near the walls but also at the center of the channel, whereas the 1D simulation shows increasing solids concentration toward the wall and very dilute flow near the center of the channel. The gas velocity vectors plotted in Figure B2 show greater interaction between the gas and clusters of particles for the 2D case.

Manuscript received Oct. 31, 2006, and revision received July 5, 2007.